IEEE Access
Multidisciplinary | Rapid Review | Open Access Journal

Received May 6, 2021, accepted May 19, 2021, date of publication May 24, 2021, date of current version June 2, 2021.

Digital Object Identifier 10.1109/ACCESS.2021.3082914

Quad-Band Multiport Rectenna for RF Energy Harvesting in Ambient Environment

SUNANDA ROY[1], (Graduate Student Member, IEEE), R. JUN-JIAT TIANG[1], MARDENI BIN ROSLEE[1], (Senior Member, IEEE), MD. TANVIR AHMED[1], (Student Member, IEEE), AND M. A. PARVEZ MAHMUD[2]

[1]Faculty of Engineering (FOE), Multimedia University, Cyberjaya 63000, Malaysia
[2]School of Engineering, Deakin University at Waurn Ponds, Geelong, VIC 3216, Australia

Corresponding author: Sunanda Roy (sunandaroy75@gmail.com)

This work was supported in part by the Telekom Malaysia (TM) Research and Development Research, Malaysia, under Grant MMUE/190001.02.

ABSTRACT This article proposes a quad-band multiport harvester that can scavenge ambient radio frequency (RF) energy of available frequency bands (i.e. GSM-900, GSM-1800, 3G and Wi-Fi) efficiently. This design's novelty is the use of frequency-dependent multiple antenna ports that enables the harvester to fully exploit all available frequency bands, spatial diversity, and polarization for maximizing the harvested RF energy at a lower power density level in an ambient environment. Indistinctly, the proposed antenna consists of 8-port which maintain $0.33\lambda \times 0.33\lambda$ (i.e. wavelength λ calculated at 0.9 GHz in free space) average area per port and has achieved more than 35% relative bandwidth (BW) with a maximum gain of 6.5 dBi to cover the selected frequency bands. Besides, the proposed quad-band rectifier with a multi-stub impedance matching network is feasible for RF harvesting over the available ambient frequency bands. The proposed rectenna's measurement results show that the generated average dc output voltage is increased up to 0.750 V at a low RF input power density of -27 dBm for a load resistance of 2.11 kΩ. The overall dc rectification efficiency of the 8-port pixel harvester is also assessed and depicted to be 66.52% when the resultant RF input power density level is -27 dBm. Measurement in an ambient outdoor and controlled indoor environment is also conducted, demonstrating that the new 8-port pixel RF harvester can produce a dc output voltage of 0.797 V which is greater than some of the reference RF harvesters.

INDEX TERMS Ambient environment, antenna measurements, multiport rectenna, quad-band, RF energy harvesting, RF survey, RF combining, rectification efficiency.

I. INTRODUCTION

The Internet of Things (IoT) assures that computers, electronic devices and other sensors will be connected to the internet so that they can become part and parcel of our network of information [1]. IoT is expected to change the way of tracking human health as well as climate, infrastructure and encourage quality, results, and improve services. In many cases, the electronic devices or sensors will be portable and wireless which need small batteries as a power source. These batteries however have a limited life span and not rechargeable and therefore arising the need and hassle of battery replacement periodically. As the IoT extends and IoT devices need to run even longer, regular battery replacements would become unsustainable and prohibitive. Energy harvesting is a promising technology to address this problem, focused on scavenging energy from peripheral sources in the outdoor atmosphere. Energy collection from the environment has been suggested for numerous energy sources, comprising light [2], temperature [3], vibration [4], and electromagnetic (EM) radio waves [5]–[8]. Nevertheless, these ambient energy sources are frequently transient and volatile, limiting the highest reliability of the scavenged fuel. RF energy harvesting has the benefit of providing omnipresent sources amongst all these combinations. Systems established on ambient RF energy harvesting often have the benefit of supplementing via wireless power transfer. Besides, it has the merit that it can offer mobility, operate at night, be inserted in walls, and be expandable to numerous nodes. A potential solution is to use rectifying antennas (rectennas) to harvest

The associate editor coordinating the review of this manuscript and approving it for publication was Giorgio Montisci.

ambient RF energy [9]. RF harvester has been used for several years in wireless power transmission (WPT) [10]. The harvester receives and transforms the EM energy that a dedicated source transmits to dc in WPT. Significant improvement has been made in WPT harvester studies [5], and there has been a further renewal because of the prospect of integrating it with mobile communication [11]. However, ambient RF energy scavenging is an additional application that uses a harvester to extract RF energy from both indoor and outdoor ambient radio frequencies [12]. The power density level of RF signals in the ambient environment has become sufficient for self-powered IoT devices with the increased number of wireless RF sources i.e. cellular networks and WiFi systems [10]. The extremely low RF power density level of the ambient environment is the main problem in RF energy scavenging, as depicted by numerous RF surveys [13]–[15]. The low RF power density severely limits the RF power that antennas receive and contributes to the rectifier's low RF-to-dc energy conversion performance. Different frequency bands, comprising GSM-900 [14], GSM-1800 [14], 3G [14], AM [16], DTV [10], and Wi-Fi [17], have been designed to extract RF energy from single-band rectennas. Various forms of antennas have been used, including dipole [18]–[20], monopole [21], loop [16], microstrip patch [22]–[25], slot [26], [27], and log-period [28] antennas. Frequency diversity has been exploited to entirely leverage the available ambient RF energy and thus multi-frequency harvesters [14], [29]–[34] and wideband harvesters [35]–[37] have been designed for the harvesting of ambient RF energy. To increase the harvested RF capacity, polarisation diversity was also considered. Both polarizations without mismatch loss can be harvested by dual linear polarized rectennas [38]–[40] and dual circular polarized rectennas [34], [35], [41], [42]. Other methods for enhancing rectenna performance or the extracted RF power have also been used, for example, harmonic rejection filtennas [43], [45]–[47], differential rectennas [34], artificial magnetic conductors [30] and so on. Using antenna arrays is a technique for extracting more RF power, notably 2-D consistent spiral antenna arrays [6], [39] and a 3-D consistent stacked bent dipole antenna array [48], and it has commonly been used in WPT [49]–[53]. For array structures, two methodologies of antenna combining are common; which are RF and dc combining, and investigation has been done on their respective advantages [54]. One inference is that the combination of dc might be more fitting for the harvesting of ambient RF energy which provides a large beam width with high gain to absorb RF signals from random directions. However, a drawback is that similar rectifiers have to rectify lower RF powers individually than they can with RF combining and lower dc rectification performance afterwards. Uniform arrays need a higher size for the rectenna array to become bulky which is a downside. The problem is that multiple antennas usually have high mutual coupling in a compact configuration [55]. In [56], different impedance matches for miniature numerous antenna systems have been addressed to reimburse for the negative effect of mutual coupling so that more RF power can be obtained in a small configuration. The use of impedance matching, however, is not optimum as it results in insertion loss and expanded complication of the circuit.

This research explains the design of an ambient RF energy harvesting multiport rectenna device where the used number of ports depends on frequency. The list of available frequency bands with associated RF input power in Malaysia is recorded from a practical RF spectral survey in Multimedia University, which is depicted in Table 4. Variation in antenna ports for harvesting RF energy at those various frequencies is a unique feature of the architecture. This makes it possible to completely use the rectenna at all available frequencies. Enhancement in available RF power density levels for a particular area along with a decrease in the required antenna matching elements are the benefits of the multiport method. This paper is structured as follows. We propose the concept of the multiport antenna in Section II with a description of a multiport rectenna device for the harvesting of ambient RF energy. In Section III, for optimizing the total RF input power, the basic layout and optimization of a quad-bands multiport antenna are calculated. The S-parameters and outcomes of radiation pattern measurement are also given. The single-port with single series diode rectifier configuration and subsequent quad-port rectifier with dc combination are provided in Section IV, and the reflection coefficient and RF-to-DC rectification performance are also provided at different input RF power density levels. Rectenna measurements for the suggested quad-band multi-port antenna and multi-bands rectifier are given in Section V. Section VI illustrates the comparisons between the proposed quad-port antenna and multiport monopole antenna for their overall RF input power and output dc power. For this article, section VII provides a conclusion.

II. 8-PORT BROADBAND FORK SHAPE ANTENNA DESIGN

The proposed wideband 8-port high-gain dual fork-shaped tuning stubs antenna structure is shown in Figure 1. The suggested antenna introduces an additional resonant stub to excite extra resonant modes and offers supplementary tuning abilities, resulting in a wider impedance bandwidth. The newly printed wide-slot (WS) antennas with two different tuning stubs are shown in Figure 1. Both of the slots were modified from the basic slot antenna with a fork-shaped stub [57]. For the typically printed WS antenna with a fork-shaped tuning stub, the slot and the feeding line was printed on the same sides of the dielectric substrate. A multi-frequency resonance technique is designed to attain a greater BW for a printed WS antenna with a fork-shaped stub. By integrating an additional fork-shaped stub (missing one arm) onto the basic fork-shaped stub and rounding the rectangular corner of the stub, excellent impedance matching (IM) over multiple operating frequency ranges was achieved. It should be noted that all the rectangular corners presented in the configuration (see Figure 1) have been changed by round corners, considering that a smooth transition contributes to

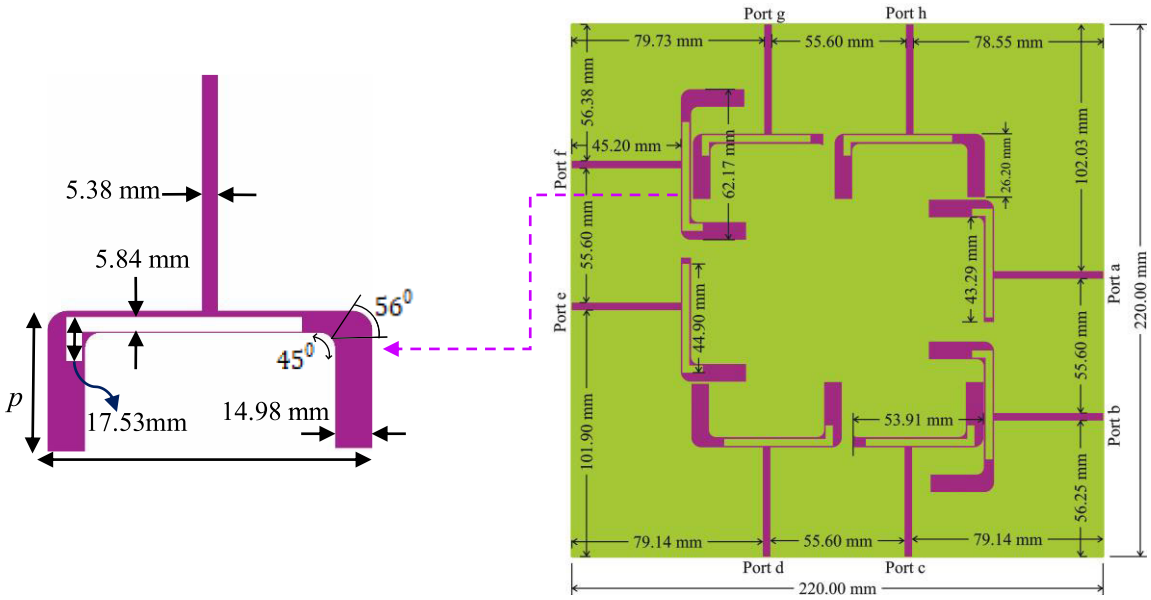

FIGURE 1. Geometrical view and dimensional details of the proposed modified fork-shaped multiband antenna.

excellent IM [58]. It is demonstrated that a half-wavelength deviation in transition current can be noticed along the boundary of the slot at the first resonant frequency [59]. The first resonant frequency f can be calculated as

$$f = \frac{300}{p\sqrt{\varepsilon_{eff}}} \tag{1}$$

With

$$\varepsilon_{eff} = \frac{\varepsilon_r + 1}{2} \tag{2}$$

Here, p is the perimeter of the stub boundary, where ε_r and ε_{eff} are the relative and effective dielectric constant of the substrate.

Each of the tuning structures is a modified version from the typical fork-shaped antenna [57]. A wideband dual stubs fork-shaped design is employed as an antenna radiating element, and 1×2 antenna array elements are arranged to create the 8-port antenna configuration. A 1×2 sub-array consists of connecting two ports on each side of the antenna using a T-junction power combiner. Similarly, four RF power combiner are connected on four sides of the proposed antenna. The 1×2 array of modified tuning stubs with the microstrip feeding line are printed on the four sides of the top layer of the dielectric substrate material. For each port of multiband antenna structure, the individual ports are marked by the notation of a-h and adjacent pairs of each side of antenna ports are RF combined to form four RF combined ports. These total number of RF combined ports are marked by the numerical value of 1 to 4 as shown in Figure 4(b). For fabricating the 8-port wideband modified dual fork-shaped microstrip feeding antenna, FR4 substrate material (1.6 mm height) with a relative permittivity of 5.4 is used.

The fabricated prototype image of the proposed antenna is shown in Figure 2. To get exact resonance in all frequency bands and improved efficiency as well as bandwidth (BW), no ground plane is assigned on the backside of the substrate. Moreover, a 50 Ω microstrip feeding line is connected to excite with each modified fork-shaped structure to develop resonance bandwidth further. The microstrip T-shaped RF power divider or combiner (Figure 3) is utilized to connect two contiguous feeding lines on four substrate material sides. The lossless T-junction power combiner can assemble RF power but has the limitations of scarcity seclusion between the output ports and an incapability to be correspondent at all ports. The displacement of antenna ports is essential for fully utilizing the rectifier efficiency at harvesting RF power for different frequency bands with associated RF power level. The proposed quad-band rectifier is not able to provide maximum efficiency for all frequency bands with associated RF power input. For example rectifier, maximum efficiency varies with the variation of input frequency bands with associated RF power level. When the rectifier is connected with a different port of the antenna, it would be able to harvest RF power efficiently from different frequency bands due to the variation of resonance response per port. That's why the same design with the different port is used for RF energy harvesting.

The T-junction power combiner is consists of a microstrip transmission line that has been divided into two transmission lines, and every line is quarter-wavelength long. When the two ports (each port is maintained at 50 Ω) of each antenna side are joined with an identical power combiner, the voltage through every leg of the combiner is of equal magnitude and phase. Four RF- combiners are used to combine 8-port into 4-ports so that the RF power of each two ports

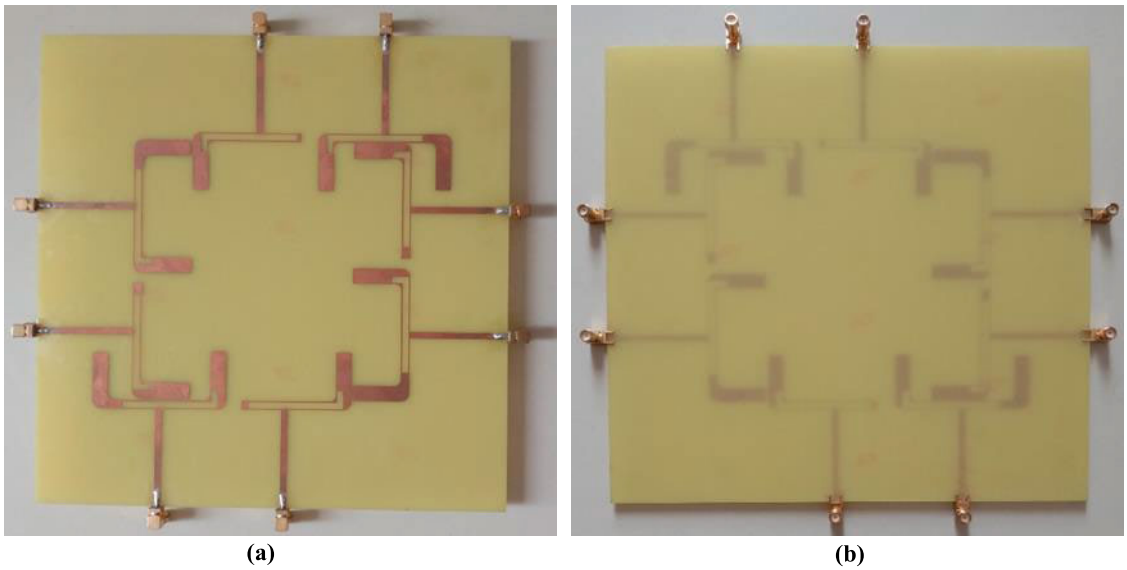

FIGURE 2. Prototype image of the proposed antenna: (a) front side and (b) back side.

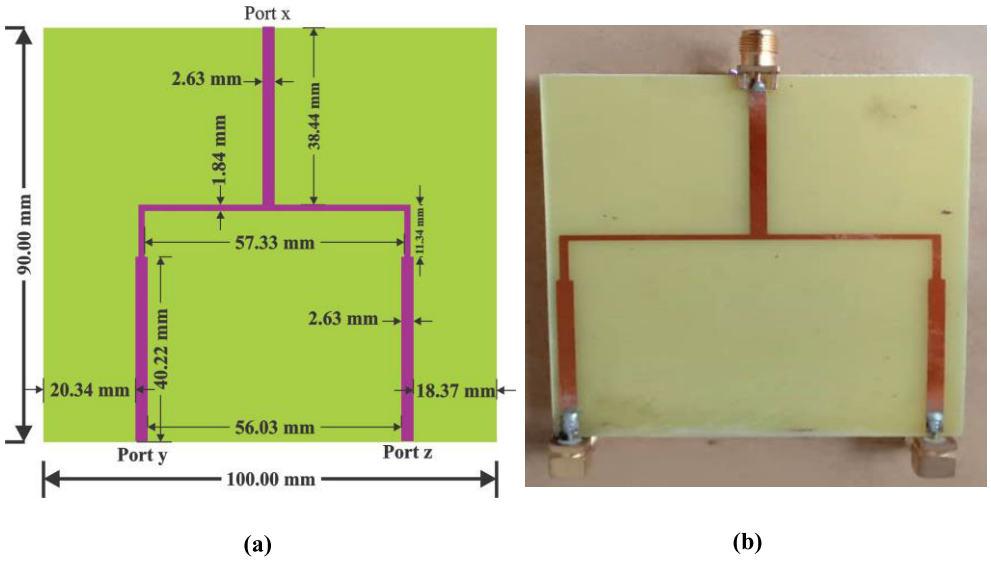

FIGURE 3. Geometrical view of the T-junction power combiner: (a) dimensional details and (b) prototype image.

is transmitted in a secured way to the rectifier section. The connection of 4 RF-combiners are aligned in the backside of the substrate so that 1) it achieves maximum isolation between each two-port of the antenna, 2) the insertion of each rectifier is also connected to the backside of the antenna thus reducing the active area of RF harvester system, 3) the RF energy scavenging system can extract RF power from all nearby directions for every 8-port antenna configuration by maintaining half-wave space. The optimized dimensions of the 8-port antenna and T-shaped RF power dividers have been determined by using computer simulation technology (CST) v19 to attain broadband operation and miniature antenna size. The average dimension of each antenna port of the suggested 8-port antenna is $0.25\lambda \times 0.25\lambda$, where λ is determined by the free space location at 900 MHz, displaying a compact 8-port antenna design.

According to the rules of selecting the center frequency of the multiband antenna, the lowest frequency of the proposed antenna is considered as a center frequency. Here GSM 900 is the lowest band within four frequency bands. But we considered the center frequency at 900 MHz for the design of the multiband antenna. If we used 940 MHz then it would have affected the dimension of the antenna as well as the gap between two ports on every side of the antenna. The average dimension of the proposed antenna for each port is evaluated in open space wavelength because the contiguous

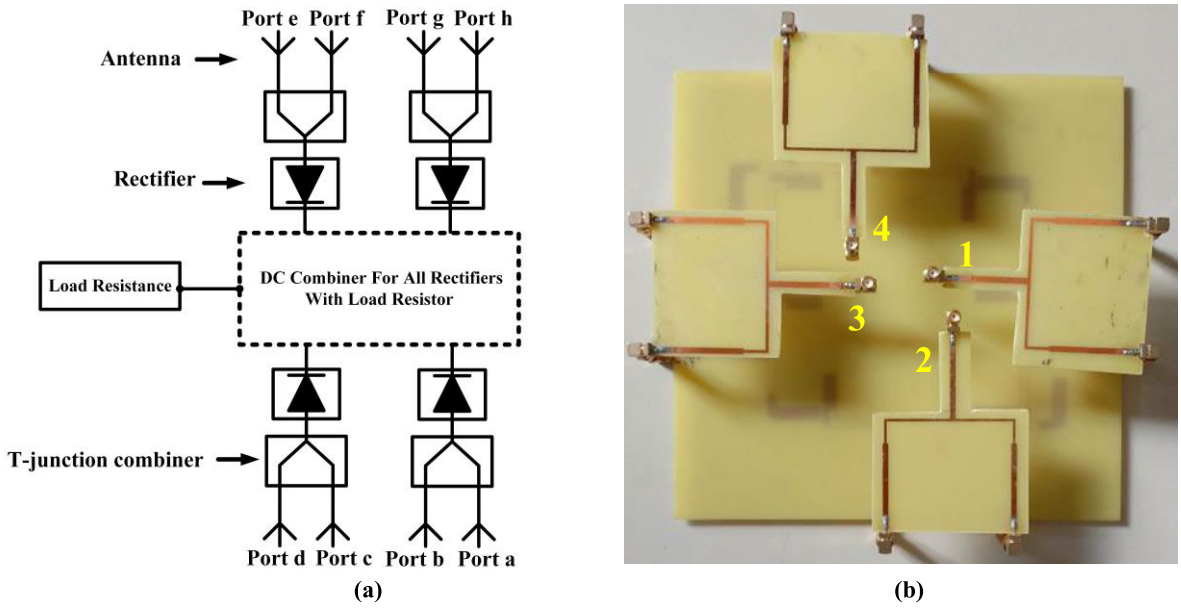

FIGURE 4. (a) DC combining process of the proposed RF harvesting technique and (b) prototype image of the integration of RF power combiner in the backside of the antenna.

antenna ports are usually coupled between them through the air.

III. MULTIPORT RF HARVESTER ARRANGEMENT

Normally two popular combining methods (i.e. RF and DC combining) combine several electromagnetic signals from multiple ports of an antenna. The RF power combining utilizes a T-junction combiner to unify the EM signal (i.e. RF power) received by every antenna port. Each of the rectifiers is employed to rectify the resultant unified RF energy. The benefit of using such type of approach is higher DC rectification efficiency owing to the strong impedance matching between the antenna ports and RF combiner. Consequently, this approach can enable the harvester to harvest RF energy with a very low RF power density level than the absence of RF combining. The disadvantage of the approach is that the narrowed down the antenna BW because RF combining affecting decreased resonances, so that it can only scavenge RF signals from a narrow range of incident directions at ambient environment. Simultaneously, in RF combining, each of the T-junction combiner's output ports is attached to a rectifier circuit and a dc combining blended the output dc power from each rectifier. Figure 4 (a) and (b) show the proposed dc combining technique and prototype image of the antenna system with backside integration of the RF T-junction combiner. The BW of dc combining is not narrowed and remains identical to that of a single port's distinct pattern, although impedance matching is essentially improved [54]. This permits the scavenging of ambient RF signals from a wider variety of incident directions compared to the RF combining process. The main drawback is that the corresponding rectifiers must distinctly rectify very low RF powers from individual ports than they would with RF combing which results in a smaller dc conversion efficiency. To overcome the limitation and achieve the usefulness of using RF and dc combining, a hybrid RF combining technique is introduced in [60]. But hybrid RF combining technique [60] enables only broad space coverage because of its single-band narrow and polarized properties. For this reason, the broadband hybrid RF combining method is proposed due to its synchronous broadband frequency range and wide space coverage area. The wideband hybrid RF combining consists of broadband RF and dc combining that is improved the impedance matching properties of RF combining which is advantageous for overcoming the limitations of dc combining. Figure 4 shows the schematic arrangement of the suggested broadband hybrid RF combining. The total number of antenna ports is 8 (port 'a' to 'h') (Figure 1) which are divided into 4 subarrays and every single subarray comprising of 2 broadband antenna ports. Firstly, two broadband antenna ports are connected by a T-junction combiner is called a subarray. Secondly, each subarray is connected with a rectifier. Finally, the output dc line of 4 rectifiers is connected by dc combining circuit. The suggested hybrid RF combining technique offers wider BW, multi-polarized RF harvesters, and wide beam width.

IV. PERFORMANCE MEASUREMENT OF THE PROPOSED ANTENNA SYSTEM

In order to verify the proposed 8-port broadband multi-frequency antenna, the prototype is fabricated Since every two contiguous ports on each side of the antenna are connected by RF combiner, the following plot shows the measured scattering parameters and the mutual couplings for 8-port of the proposed antenna. The comparison between

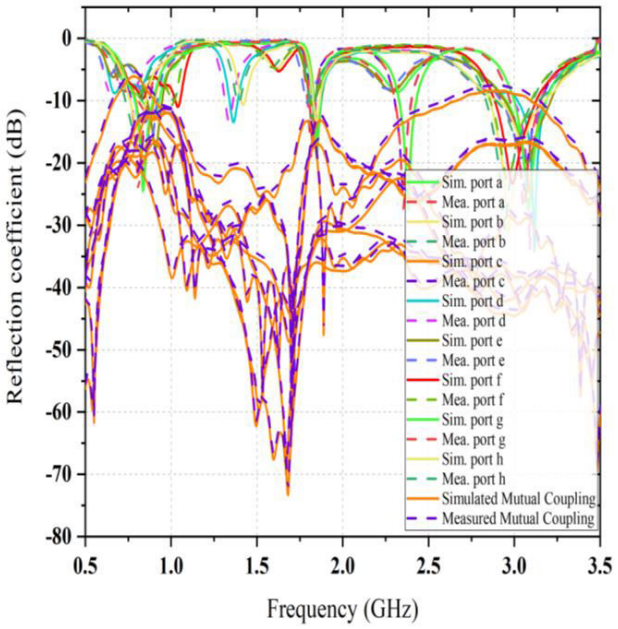

FIGURE 5. Simulated and measured reflection coefficient and mutual couplings of the proposed antenna between ports a-h.

simulated and measured reflection coefficient and mutual coupling of the proposed antenna is shown in Figure 5. It can be seen that there is a good agreement between simulated and measured performance and measured results are shifted toward the lower frequency region in comparison with the simulated result. The S-parameter and mutual couplings of the multiport antenna are measured by an Anritsu MS2024A VNA Master handheld Vector Network Analyzer. The measured S-parameters of the port a-h are less than −10 dB from 800 MHz to 3 GHz, achieving a wide relative BW of 48%. The measured mutual coupling between every two adjacent ports in every side of the antenna from port 'a' to 'h' is less than −12 dB over different frequency bands (i.e. GSM 900, GSM 1800, Wi-Fi and LTE) so that every portable combined antenna can scavenge RF energy individually.

There are several reasons to maintain excellent isolation among the antenna ports such as 1) fork shape feeding lines achieving spatial diversity (i.e. port a and port b), (2) proper spacing between each antenna port attaining phase diversity (i.e. every adjacent from port a to port h) and (3) the connection of same RF combiner for each adjacent port in backside alignment of the antenna achieving good matching and angular diversity, (e.g. port a and h). Generally, the measured scattering parameters and mutual coupling performances depict that the 8-port multiband antenna has achieved excellent impedance matching and incoherency across the available frequency bands in the ambient environment. The measured E-field and H-field radiation patterns of the suggested antenna for the port of a to h excitation (50 Ω load is connected in one port when taking measurements in other port) at different frequency bands (i.e. 0.95 GHz, 1.81 GHz, 2.42 GHz and 2.90 GHz) are shown in Figure 6. The proposed antenna's E and H-field radiation patterns are denoted by the y-z plane as vertical polarization (i.e. when $\Phi = 90$) and x-z plane as horizontal polarization (i.e. when $\Phi = 0$) respectively. The same Master Network Analyzer is used to measure the co-pol and cross-pol radiation patterns at control environment. It can be seen that both co-pol and cross-pol of the H-field are less than the E-field's co-pol and cross-pol situated at the centre of the polar form. In each field (i.e. E-field and H-field), the radiation pattern (i.e. co-pol and cross-pol) is intersected. The cross-polarization of both fields (i.e. E and H) is perpendicular to the desired linear direction for most of the antenna ports which is an excellent antenna characteristics. Due to the identical design, port *b* and *d* have a closely similar radiation pattern to port *f* and *h* and port *a* and *c* have an approximately similar pattern to port *e* and *g* for each frequency band so that the total harvested RF energy can be increased. It shows that lower frequency regions exhibit dual-polarized radiation patterns both fields (i.e. E and H) of co and cross-pol. The benefit of having a dual linear polarization pattern is that it can harvest all the energy from arbitrarily polarized incident waves without polarization mismatch loss. With the increasing frequency bands, the radiation pattern for H-field (co and cross-pol) turn into omnidirectional or isotropic. Here, at 0.94 GHz, 1.81 GHz, 2.42 GHz and 2.90 GHz, the co-pol radiation of antenna ports a to h are linearly polarized in the vertical direction which presents the ability to scavenge ambient RF energy from available frequency bands without any polarization loss.

The total radiation efficiency of the prototype for each port is shown in Figure 7(a). The measured maximum total radiation efficiency of the ports a, d, e and h are around 74.09 %, 67.27 %, 71.93 %, 65.29% across 1.81 GHz; port c and g around 77.41% and 77.90% over 2.42 GHz, and port b, f about 73.70%, and 71.77% over 2.9 GHz demonstrating better impedance matching, isolation and better radiation efficiencies. The comparison between simulated and measured gain of the proposed antenna is presented in Figure 7(b). It shows that the measured and simulated gain has a good agreement due to the fork shape feeding element and good impedance matching for each antenna port. The measured realized gains of the antenna ports *a* to *h* are around 3.2 dBi over GSM 900, 3.7 dBi through GSM 1800, 3.5 dBi through Wi-Fi and 7.6 dBi over 2.9 GHz indicating high antenna realized gains which are helpful to scavenge RF energy of very low RF power levels with decent dc rectification efficiency. The omnidirectional directional radiation pattern of the proposed antenna for each port is presented in Figure 6. The advantage of the omnidirectional pattern is that it has realized a gain over 3.5 dBi thus the received EM energy can be improved resulting in better dc rectification efficiency even though the available RF power density is very low in the ambient environment. Every port of the multiport antenna can scavenge RF power from only half-space diversity.

Every 8-port antenna configuration offers four realized gain (i.e. above 3.5 dBi) beams involving a half-space

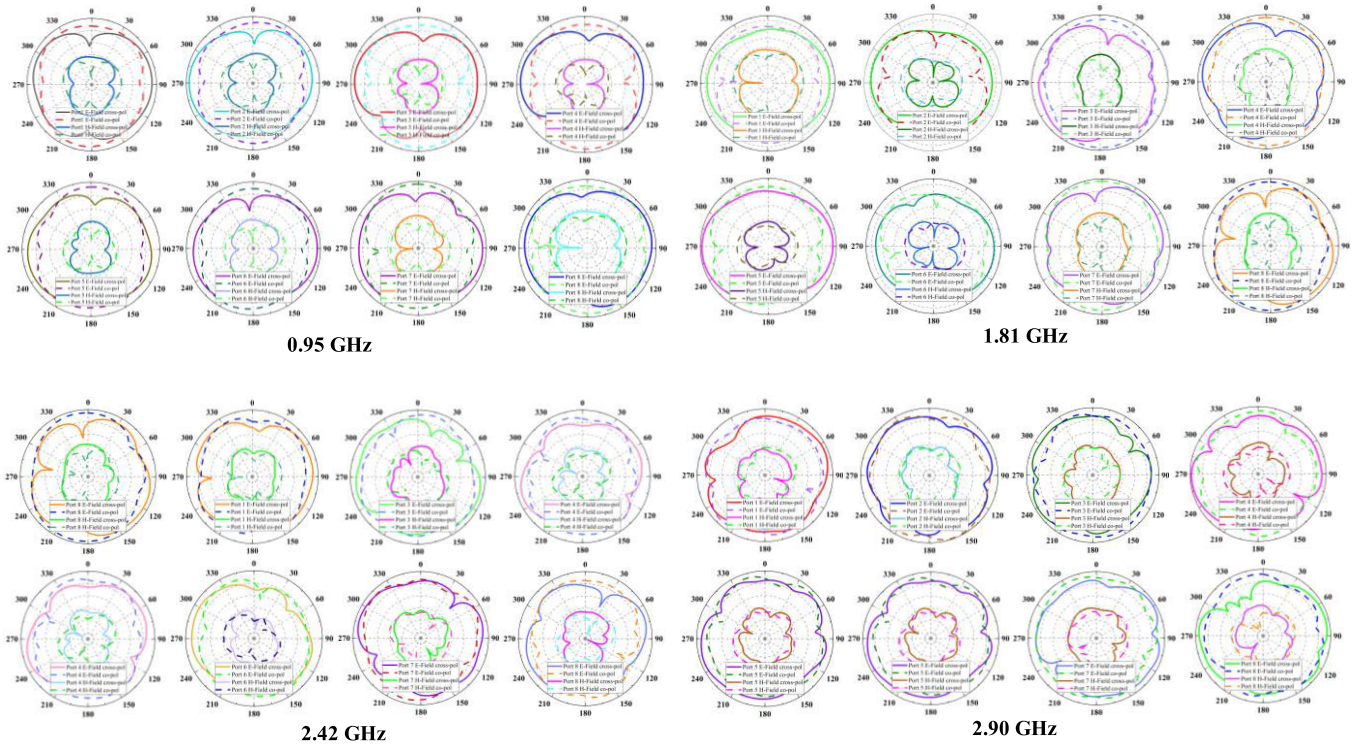

FIGURE 6. Measured E-Field and H-field radiation pattern (cross-pol & co-pol) of the port a - h in the fork-shaped wideband antenna for the different frequency bands.

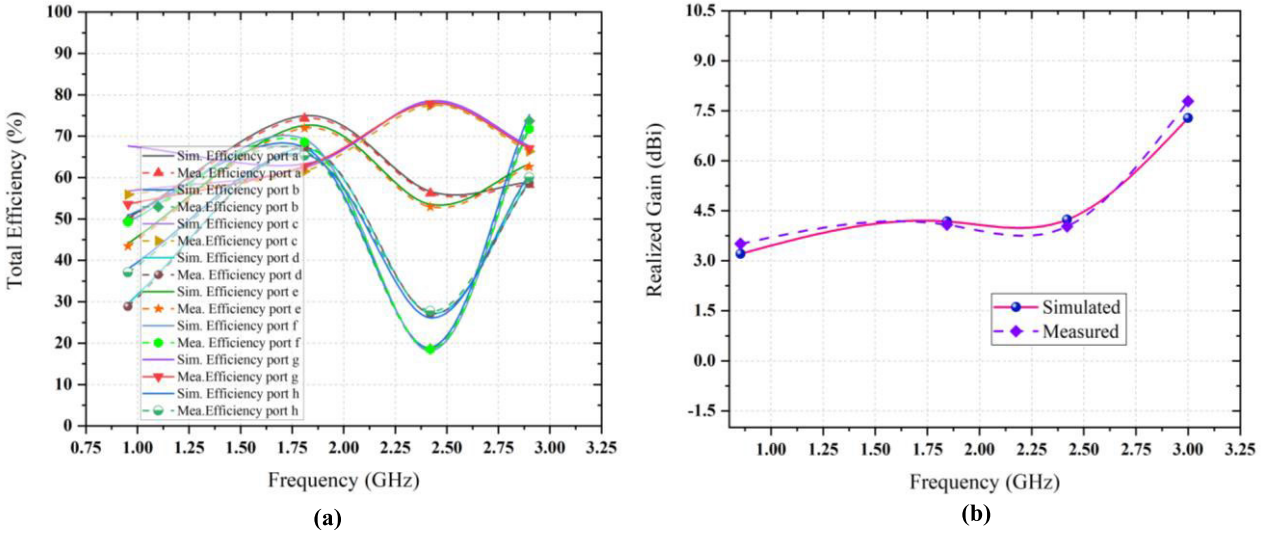

FIGURE 7. Comparison between the simulated and measured (a) total efficiency per port (i.e. *a* to *h*) and (b) gain of the proposed antenna.

diversity so that the suggested 8-port fork shape antenna has in total eight realized gain wide beams while it can scavenge RF power from all available directions with better isolation. A 1 × 2 sub-array consists of connecting two ports on each side of the antenna using a T-junction power combiner. Similarly, a 1 × 4 array can be formed by connecting four RF power combiners on four sides of the proposed antenna. The prototype combination of such design is shown in Figure 4(b) where an RF power combiner exists in the proposed antenna's backside. This way, the array combination has more flexible and reliable to connect multiband rectifier so that every output port (port x) of the RF power combiner can harvest energy independently. The simulated and measured scattering parameter of the output port of the power combiner is

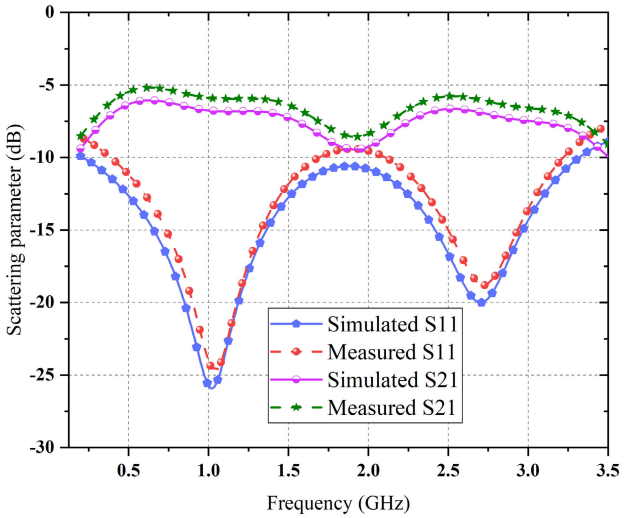

FIGURE 8. Simulated and measured the scattering parameter of the output port (port x) of the sub-array.

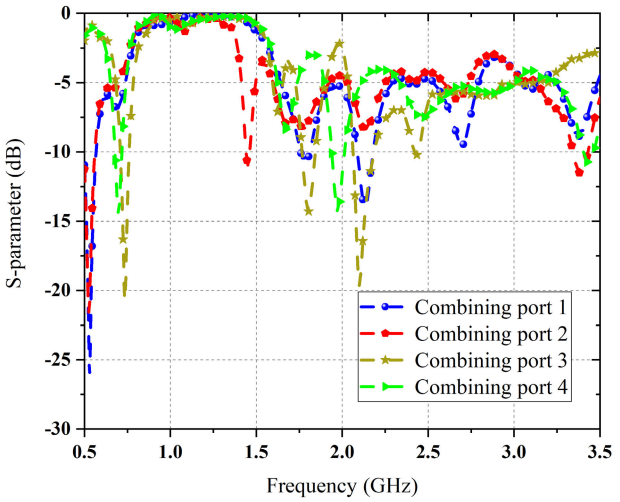

FIGURE 9. Measured reflection coefficient of the four combined ports of proposed antenna.

illustrated in Figure 8. It can be seen that the measured scattering parameter is less than 10- dB from the 0.9 GHz to 2.9 GHz frequency range which can still cover the GSM-900 and LTE bands. In Figure 9, it is shown that the measured reflection coefficient of four combined port of the antenna which is demonstrated in Figure 4(b). It should be noted that the measured reflection coefficient is efficient for available frequency bands at ambient environment.

V. MULTI-BAND RECTIFIER DESIGN

A. MULTI-BAND RECTIFIER DESIGN

The suggested multiband rectifier topology for GSM 900 and 1800, Wi-Fi and LTE bands are depicted in Figure 10. It is the stage one half-wave rectifier. The single series diode rectifier consists of a matching network and an RF-to-dc converter in

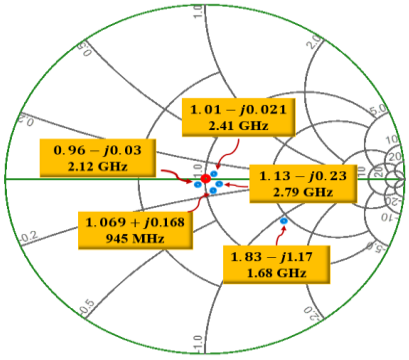

FIGURE 10. The proposed multi-band rectifier topology.

which a Schottky diode, Avago HSMS-2850 was selected as the optimal solution for our ambient RF energy harvesters.

However, it is too small to provide a ripple-free dc voltage to the load. This can be overcome with a matching network that will allow a good impedance match with a large output capacitor but at the expense of introducing losses. The rectifier circuit's main parts are an impedance matching network (IMN) (consisting of various microstrip rectifying elements such as short stubs, open stub, radial stub and transmission line), a Schottky diode, a low pass filter or a single capacitor and a load section. A single series diode rectifier circuit is selected due to higher RF-to-dc rectification efficiency at a very low-level ambient RF input power density compared to other rectifier topologies such as single shunt diode [36], voltage doubler [6], and Greinacher [57], [54]. Moreover, a harmonic balance solver (HBS) of an advanced design system (ADS) is used to evaluate the proposed rectifier topology's performances. The 1.6 mm thick FR4 has a relative permittivity of 5.4, and a dissipation factor of 35 as the substrate material decreases the insertion loss and prefers the Avago HSMS-285B diode with a small switch-on voltage as a dc-rectifying Schottky diode to increase the RF-to-dc conversion efficiency at a low RF level.

The prototype image of the fabricated rectifier topology is presented in Figure 11. The input impedance of the rectifier for the different frequency bands with input RF power of −20 dBm are 1.069+j0.168@945 MHz, 1.83-j1.17@1.68 GHz, 0.96-j0.03@2.12 GHz, 1.01-j0.02@2.41GHz and 1.13-j0.23@2.79 GHz as shown in Figure 12. The value of load resistance is significant to the RF rectifier design because it delivers a dc offset voltage for the quad-band rectifier, which affects the dc-rectification efficiency

In order to get maximum dc rectification efficiency of the proposed multi-band rectifier, it has been tried to synchronously maximize the dc conversion efficiency at different frequency bands for a very low input RF power density level. Consequently, by applying HBS in ADS, the optimal value of load resistance from 0.5 kΩ to 10 kΩ with a period of 0.25 kΩ is found and the dc rectification efficiency is optimized at the available frequency bands under the low ambient input

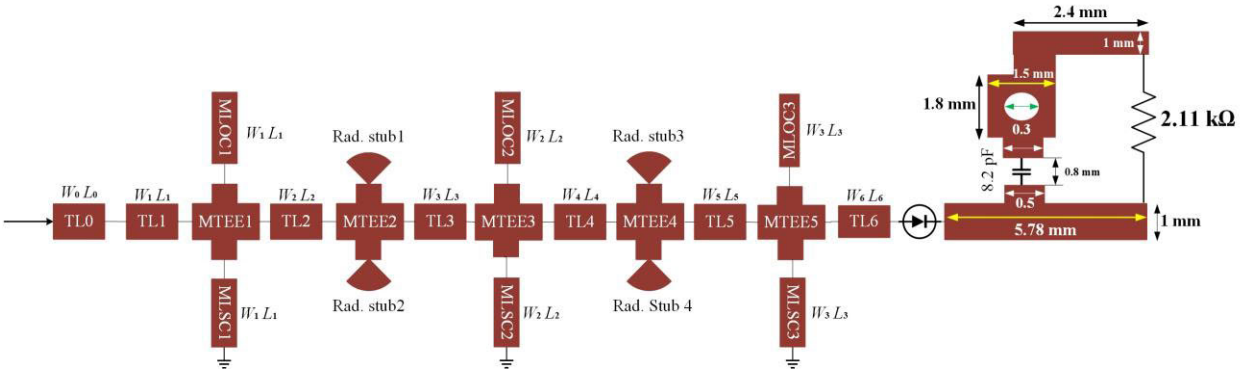

FIGURE 11. The prototype image of the suggested multi-band rectifier circuit.

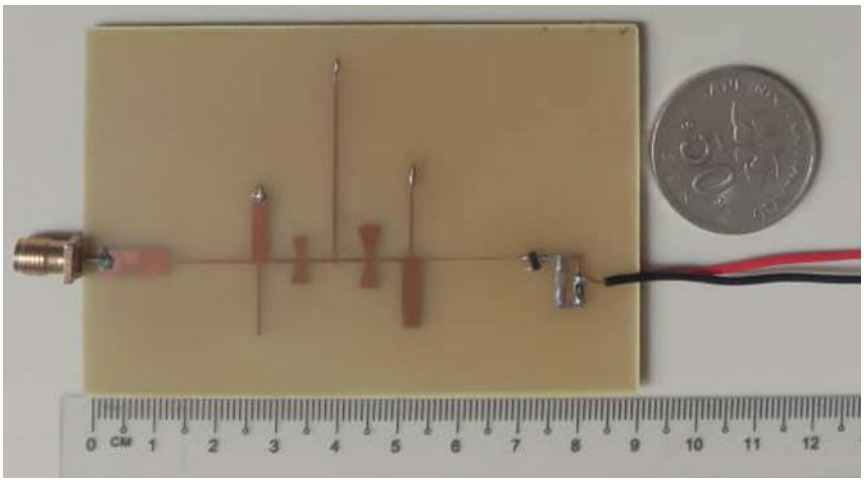

FIGURE 12. The impedance of the rectifier for different frequency band for the RF input of −20 dBm.

RF power level of −27 dBm for individual load value. The comparison between simulated and measured dc rectification efficiency of the rectifier as a function of load resistance for ambient RF power of −30 dBm at multiple frequency bands (i.e. GSM 900 and 1800, 3G, Wi-Fi and LTE) is shown in Figure 13. It can be seen that the dc-rectification efficiency at different frequency bands varies with the values of load resistor and the maximum conversion efficiency is achieved at about 2.11kΩ. To choose the best value of load resistance as long as it is achieved the highest dc conversion efficiency over the five frequency bands. As presented in Figure 13, the selected optimal load resistance of the multi-band rectifier is 2.11 kΩ. From the equations (3), it is demonstrated that rectification efficiency is directly proportional to the square of generated dc voltage and inversely proportional to the load impedance. That means the lower the value of load resistance higher the conversion efficiency. In order to get higher conversion efficiency, impedance matching network and rectifier topology should be designed in such a way that the rectifier generates higher dc voltage with a lower value of load resistance. Designing and optimizing the perfect IMN is difficult in that 1) the impedance between antenna and rectifier is complex and conjugal to each other, 2) the available bands of frequency are neighboring in the frequency spectrum, and 3) input impedance of the suggested rectifier is varied due to the nonlinear behavior of the diode and the effect of low-level RF power density. To overcome the difficulties, the multi-stubs microstrip elements are used to design the impedance matching network to adapt different frequency bands, as presented in Figure 10. It can be seen that the proposed multi-stub IMN consists of multiple single-stub tunings (i.e. open stubs, short stubs and radial stubs) in cascade connection. In Figure 10, there are five sets of microstrip rectifying elements: MLOC1, MLSC1, MLOC2, MLSC2, MLOC3, MLSC3, Radial Stub1, Radial Stub2 and Radial stub3. Moreover, within five sets of microstrip elements, the first three sets consist of an open-circuited stub (MLOC) and a short-circuited stub (TLSC) and another two sets consist of Radial Stub only. The combination of open and short stubs offers a frequency-reliant resistance with fourth degrees of liberty to recompense the input impedance's imaginary section at the joining point. TL0, TL1, TL2, TL3, TL4,

TABLE 1. The optimized dimension of various rectifying elements of the matching network of the rectifier.

Rectifying element	Length (L)mm	Wide (W)mm	Rectifying element	Length (L)mm	Width (W)mm
TL0	10.75	3.925	MLSC3	13.561	0.565
TL1	13.7	0.5	TL5	5	0.625
MLSC1	10.614	2.528	MLOC3	10.72	3.035
MLOC1	11.78	0.68	TL6	5	0.625
TL2	5	0.625	TL7	17.47165	0.256
MLSC2	31.064	0.7227	Radial Stub 1	3.35	1.125 Angle (35^0)
TL3	5	0.625	Radial Stub 2	3.5	0.312 Angle (36^0)
MLOC2	0.5	0.5	Radial Stub 3	4.22	0.925 Angle (35^0)
TL4	5	0.625	Radial Stub 4	5.32	0.787 Angle (35^0)

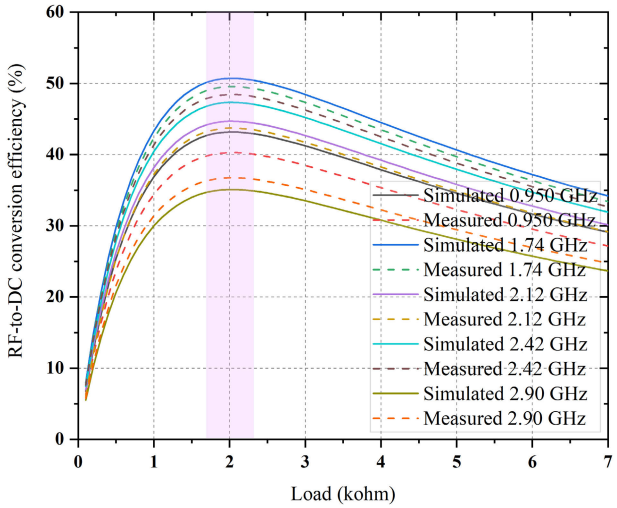

FIGURE 13. Comparison between simulated and measured RF-to-dc rectification efficiency of the rectifier versus load values (K-ohm) at an input RF power of −27 dBm over different frequency bands.

TL5 and TL6, which join the matchless rectifier and the sets of transmission line stubs, are applied for the microstrip transmission line impedance modification so that the real part of the input impedance can be progressively changed to the typical impedance for example 50 Ω. The pair of microstrip rectifying elements are aligned such as MLOC1 and MLSC1, MLOC2 and MLSC2, MLOC3 and MLSC3, Radial Stub1and Radial Stub2, Radial stub3 and Radial stub 4, and TL0 to TL6 to form the multi-stub IMN. The total number of freedom is 24 degrees to attain a quad-band impedance adapting covering the available bands of frequency such as GSM 900 and 1800, Wi-Fi and LTE, respectively. TL0, a microstrip element with 50 Ω characteristic impedance is used for subminiature (SMA) RF connector soldering. Moreover, MLSC1, MLSC2, and MLSC3 are connected with the ground to deliver dc bias in the rectifier circuit. The lengths and widths of various rectifying elements in the multi-stub IMN are optimized using ADS for realizing excellent quad-band impedance adapting and a miniature rectifier active area. The optimized values of various parameters of the rectifying elements of IMN are presented in Table 1.

B. MEASUREMENT OF PROPOSED RECTIFIER

In order to verify the proposed multiband rectifier, a prototype is fabricated. The dimension of the multiband rectifier is 74 mm × 51 mm. The comparison between simulated and measured reflection coefficient at various input RF power density levels is shown in Figure 14(a). There is an excellent agreement between simulated and measured scattering parameters due to the benefit of the optimized IMN. It can be seen that the proposed rectifier covers the desired five frequency bands for various RF input power levels of interest. Figure 14 (a) shows five resonance frequencies (i.e. GSM 900 and 1800, 3G, Wi-Fi and LTE), which are shifted slightly with the variation of RF input power density level at −35 to −15 dBm.

Regardless of frequency shifting, the excellent impedance matching at various bands of frequency such as GSM 900 and 1800, 3G, Wi-Fi and LTE of the multiband rectifier at available low RF power level of −35 dBm to −15 dBm, presents the effectiveness of the impedance matching network which consists of microstrip multi-stub elements. Moreover, the unknown parasitic behavior of the SMD components in the circuit affects the shifting on the reflection coefficient. The exact value of the chip capacitor is normally a function of frequency. To reduce the influences, products with similar values but different series numbers can be used to replace the components. To estimate the dc rectification efficiency, a signal generator is connected to the rectifier's input section, and a multimeter is used to estimate the generated dc voltage over the load section. The following equation determines the

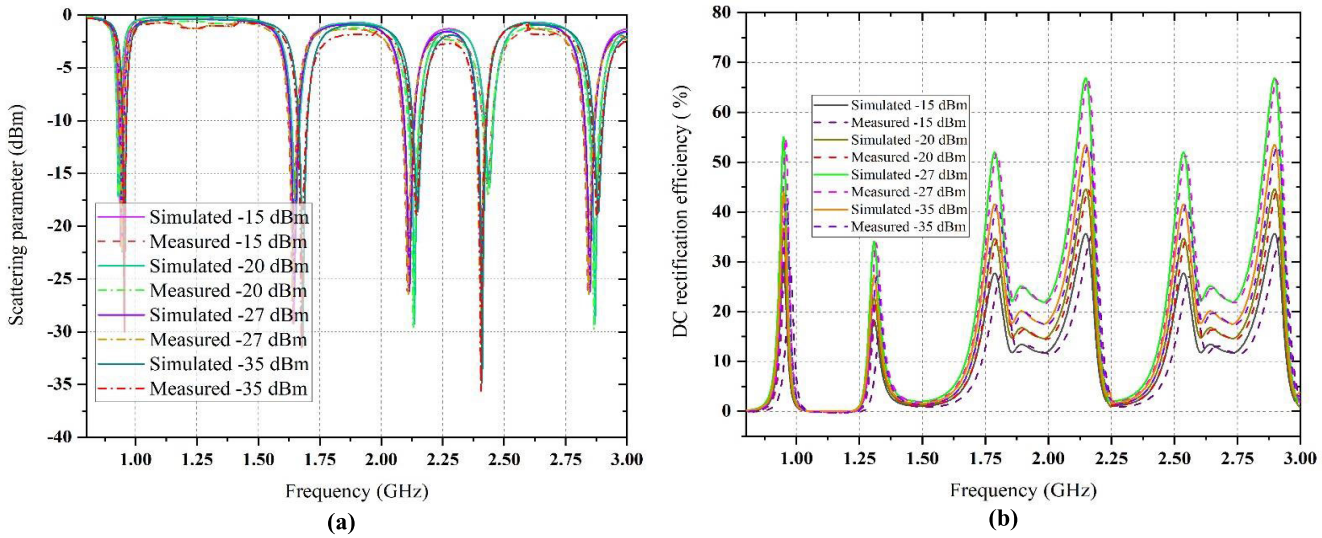

FIGURE 14. The simulated and measured (a) scattering parameter versus various RF power density levels and (b) dc rectification efficiency versus frequency for different RF power density levels of the multiband rectifier.

RF-to-dc rectification efficiency:

$$\eta = \frac{V_{dc}^2}{P_{RF@input}.R_L} \tag{3}$$

where, $p_{RF@input}$ is the input RF power supplied by the signal source, and V_{dc} is the dc output voltage over the load impedanceR_L.

The comparison between simulated and measured dc rectification efficiency as a function of frequency for four RF input power density levels is depicted in Figure 14 (b). At the same RF power density level, it can be seen that the efficiency at GSM 900, 3G and LTE is greater than the efficiency at frequency GSM 1800 and Wi-Fi. This is due to higher loss of diodes and PCB at GSM 1800 and Wi-Fi frequency bands. It can be seen that the efficiency over the frequency bands of interest is well maintained for different RF input power density levels. Due to the benefit of the optimized IMN, the measured dc rectification efficiency is in good agreement with the simulated dc rectification efficiency without major discrepancies. The maximum dc rectification efficiency at GSM 900 and 1800, 3G, Wi-Fi and LTE bands were 55.5%, 52.5%, 66.52%, 52.9% and 65.5 % for −27 dBm and 44.2%, 41.2 %, 54.1%, 41.0% and 54.0% for −35 dBm, respectively, representing better dc conversion efficiency at available bands of frequency at ambient low RF power density levels. To depict the advantage of multiband operation, an RF combiner is used to merge the single-frequency signals at various frequencies delivered by several signal sources and inputting the merged multi-tone signal into the proposed rectifier. It can be observed that the phase difference among single-frequency signals influences the dc conversion efficiency as described in [62]. Moreover, the optimization of the phase for multi-tone signals is not optimized because the phase of different frequency signals varies randomly in the ambient environment.

The comparison between simulated and measured RF-to-dc rectification efficiency versus different RF power density levels for the input frequency signals is presented in Figure 15. It can be seen that the RF-to-dc rectification efficiency increased with an increased number of input signals and reached 64% as maximum. This is due to a good impedance adaptation between the antenna and IMN section of the rectifier and an almost perfect dc sum. If some of the incident powers don't have the same value, the impedance matching, and therefore, the RF-to-dc rectification efficiency, is not optimum. The multi-tone input signal (i.e. GSM 900 and 1800, 3G, Wi-Fi and LTE) has the maximum dc rectification efficiency three times greater than the dc conversion efficiency of each single-tone input signal of −35 dBm RF power density level. The achieved maximum dc rectification efficiency is due to several RF power being collectively received from the broad bandwidth.

In Figure 15, the resultant RF input power can be observed by multiplying several numbers of signals with RF input power in each signal. As a matter of fact, with identical RF input power per signal, a rising number of signals will enhance the sum of RF input power. Moreover, the amount of harvested RF power from the multiband antenna is greater than the single-band antenna with all available ambient frequency bands. Therefore, Figure 15 illustrates the advantage of the multi-band performance in ambient RF power scavenging in which the dc rectification efficiency and the dc output voltage can be enhanced.

The rectifier has achieved higher RF-to-dc rectification efficiency compared with past relevant works in the multiple frequency spectrums (i.e. GSM 900 and1800, 3G, Wi-Fi and LET) at very low-level RF power density

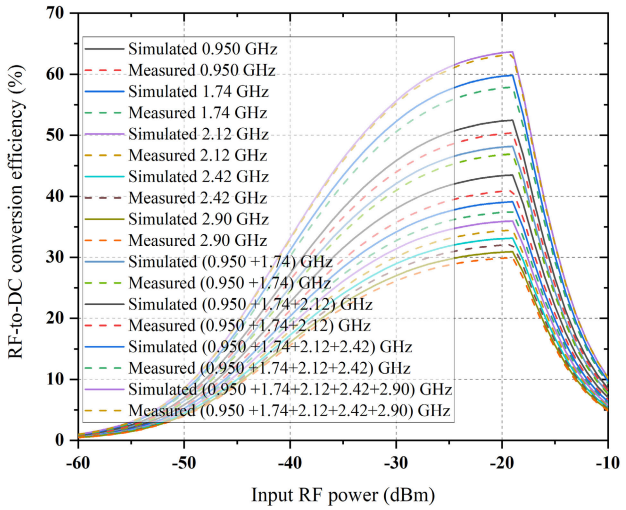

FIGURE 15. The simulated and measured RF-to-dc conversion efficiency VS different RF power density levels for input frequency signals.

(i.e. −30 dBm to −15 dBm), presenting the benefit of the multiband rectifier design approach. The dc rectification efficiency rises with the ambient RF power level because of the enhancement in received RF power.

VI. MEASUREMENT OF MULTIPORT RF HARVESTER

A. PROTOTYPE IMPLEMENTATION OF MULTIPORT RF HARVESTER

Prototype hardware is fabricated to verify the performances of the proposed multi-frequency RF harvester. The front and back side image of the prototype is depicted in Figure 16 (a) and (b). To fabricate the RF harvester prototype, a wideband 8-port antenna, four RF power combiners and four multi-band rectifiers without load resistor are fabricated and used. The 8-port RF harvester consists of 8-port antenna configurations assembled back to back with four RF power combiners and four multi-band rectifiers to decrease the multiband harvesting system's effective area. To execute the multiport harvesting system, RF power combining is implemented in the 8-port broadband fork shape patch antenna by connecting four T-junction RF power combiners and then RF-to-dc combining is accomplished by summing the output dc voltage from the four multi-band rectifiers which are associated to four RF joined ports. The generated output dc voltage of each rectifier is then joined in a shunt to raise the dc output current.

For every 8-port antenna system, four multiband rectifiers are joined to the four T-junction RF power joint ports. Due to sharing of the same ground plane of the four rectifiers, the dc output voltage is connected in series that will short circuit the diodes connection. It should be noted that amount of dc voltage is increased because of the series connection. Finally, the output DC and voltage are increased due to the parallel and series connection of dc outputs. When the four multi-band rectifiers' dc outputs are combined, the resultant load impedance should be altered depending on the combining criteria. Therefore, the outputs dc of the four multi-band rectifier is connected in parallel and series respectively, the resultant load impedance for the multiband ambient rectenna system is chosen to be $R_L = 2.15\ k\Omega$ according to [8], [63].

B. MEASUREMENT IN THE LAB ENVIRONMENT

The performance of the proposed quad-band ambient RF energy harvesting system is measured in a controlled environment, which is shown in Figure 17. In Figure 17(a), it is demonstrated the measurement technique at applied lab in MMU. The multi-tone signals are generated by using an RF power combiner to combine the single-tone signals at different frequencies provided by multiple signal generators. Then, a power divider is used to split the multi-tone signal into two equal-power multitoned signals to feed two dual-polarized horn antennas, which are placed at both sides of the proposed energy harvesting system. For each dual-polarized horn antenna, another power divider is used to split the multi-tone signal into two equal-power multi-tone signals to feed the horizontal-polarized and vertical-polarized antenna ports. The proposed energy harvesting system is placed between the two dual-polarized horn antennas and it is in the far-field regions of the two dual-polarized horn antennas to harvest the multitoned dual-polarized incident waves from two opposite directions. It should be noted that the multiple tones and two polarizations are simultaneously excited as incident waves, and are used to simulate the ambient RF energy simultaneously distributed in different frequency bands (due to multiple wireless communication systems including GSM 900, GSM 1800, 3G, and WiFi) and different polarizations (due to the scattering, reflection, and diffraction of the wireless channel). The RF power received by each antenna port is measured by a spectrum analyzer. The multiple frequency signals are adapted so that the power received by the multiband antennas, is similar to make sure that the multiband rectifiers can operate with better dc conversion efficiency at all available frequency bands [14], [31], [65]. Then we connect the rectifiers to antenna ports and use a multi-meter to measure the output dc voltage to find the output dc power and RF-to-dc efficiency. The measured output dc voltage and power of the proposed energy harvesting system for different multi-tone input signals are compared with those of the single-tone, as shown in Figure 17(b). We evaluate the performance of the proposed energy harvesting system versus the power density because it reflects both the performance of the antenna and rectifier in the entire system. The multiple signals are produced by employing a T-junction RF combiner to merge the single frequency signals at multiple frequencies generated by the signal generator. The Anritsu MS2024A Master Vector network analyzer (VNA) is used to measure the received power by every antenna port, and the Friis formula is used to calculate the transmitting power, and distance between the transmitting and the receiving antenna [64]. Four rectifiers are then connected to the two antenna ports of each side

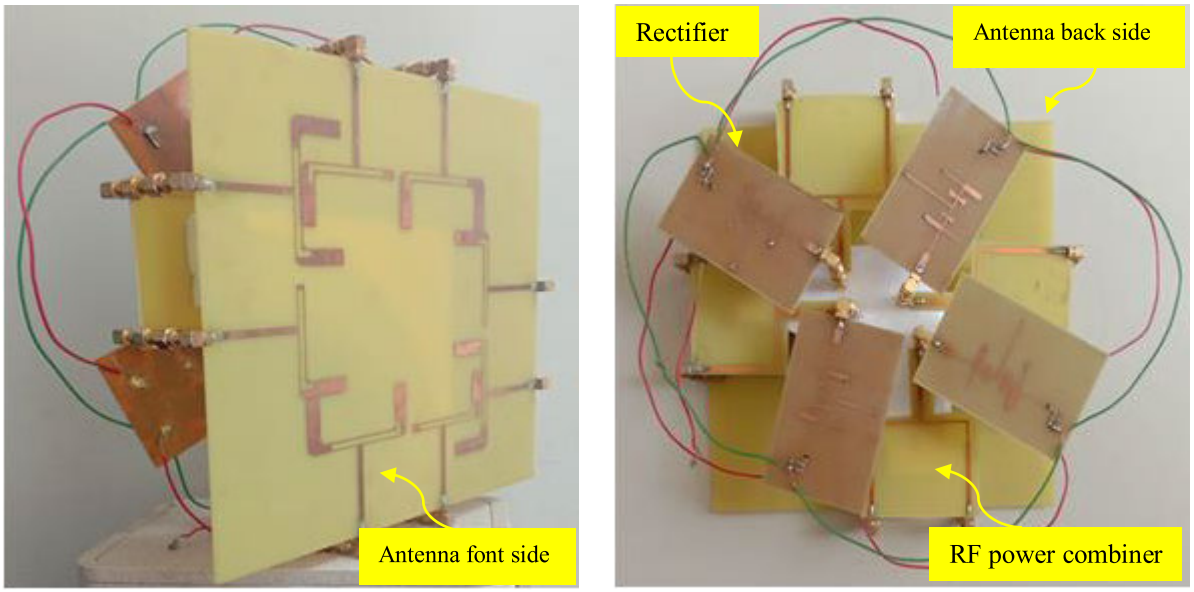

FIGURE 16. The prototype of the multiport RF energy harvester (a) front side (b) backside.

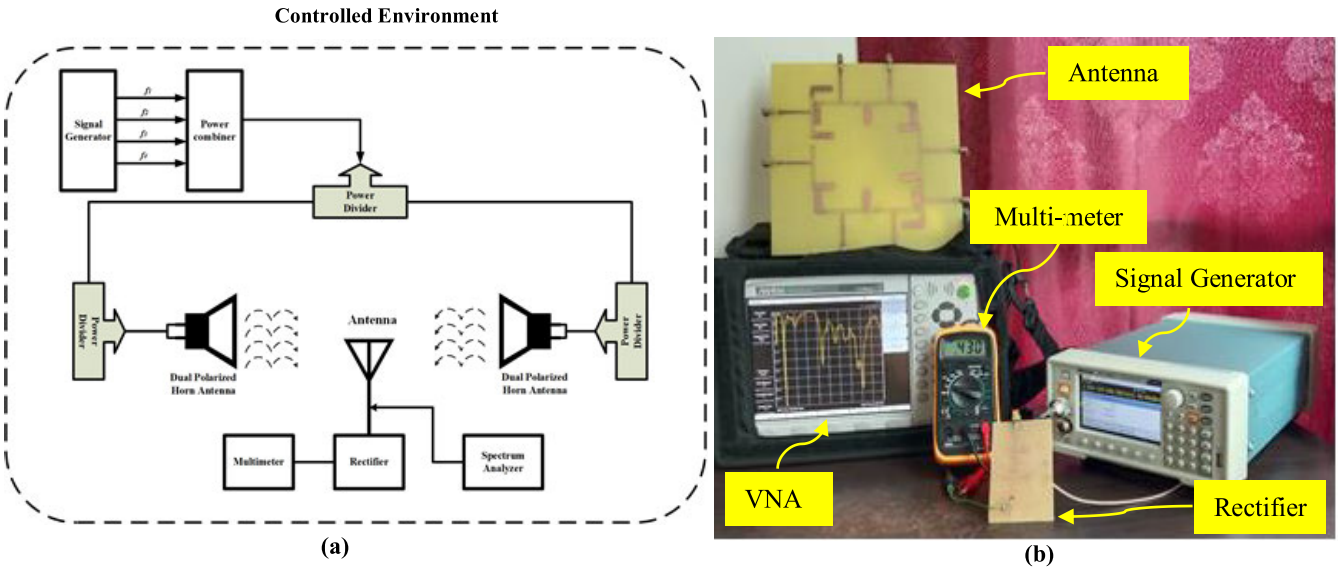

FIGURE 17. Measurement (a) technique and (b) performance in the proposed rectenna in the lab.

through the dc combining, and a multi-meter is employed to determine the resultant dc output voltage. It should be noted that the multi-frequency signals are concurrently excited as exploit waves, and are employed to simulate the RF power which is disseminated in various frequency spectrums such as GSM 900 and 1800, 3G, Wi-Fi and LTE respectively. The comparison between simulated and measured voltage (i.e. output dc voltage) of the suggested rectenna for a variety of frequency signals is shown in Figure 18.

The overall generated dc voltage of the harvester depends on the dc conversion efficiency and RF input power density level. The multi-tone RF input signal (0.950 GHz, 1.81 GHz, 2.12 GHz, 2.42 GHz and 2.90 GHz) has the maximum output dc voltage amid all the scenarios. The multi-frequency input signals can generate more dc output voltage than the single frequency input signal with ambient RF power density level, illustrating the benefit of the proposed multiport rectenna system's multiband operation. The multi-band operation is able to receive additional RF power from both indoor and outdoor ambient environments where RF energy is scattered in available frequency spectrums to deliver more dc output voltage. Moreover, multi-frequency input RF signals can raise the dc rectification efficiency contrasted to the single-frequency input signals because of additional RF power being accepted

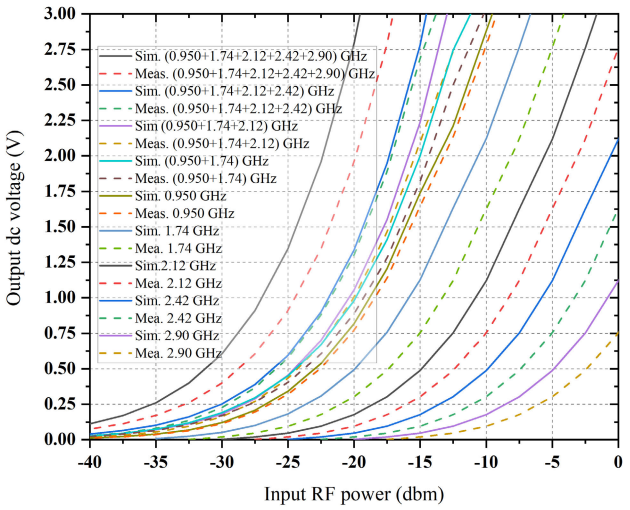

FIGURE 18. The comparison between simulated and measured output dc voltage of the suggested rectenna system as a function of RF power density level for different frequency input signals.

from the broad BW. Mainly, the measured dc output voltage is larger than 0.400V with the input of −30 dBm power level, and the dc rectification efficiency is larger than 66.52% when the RF power density level is less than −20 dBm. The proposed RF energy harvesting system has achieved 0.350V output voltage when the associated RF power density level is −20 dBm with 44.2% RF-to-dc rectification efficiency. A comparative study is illustrated between the proposed rectenna and previous related work in terms of RF input power density level, harvested dc output voltage, RF-to-dc rectification efficiency, as presented in Table 2. It can be seen that the proposed new RF harvester offers maximum output

TABLE 2. The performances between new and previous relevant work.

Ref.	RF Input Power, dBm	DC output voltage, mV	DC rectification efficiency (%)
[14]	-16.0	225	40
[31]	-11.0	470	25
[36]	-18.0	300	40
[64]	N/A	N.A.	2.3
[68]	-10.9	570	40
[66]	-11.4	1555	3
New	-27	797	66.5

dc voltage as well as RF-to-dc rectification efficiency with associated very low RF power density levels in comparison with past related researches.

Such excellent performance of the proposed rectenna is achieved because of better antenna gain, simultaneous exploits of different frequency signals and circular polarization to enhance the RF input power density levels as presented in Table 3. A more detailed, comprehensive analysis is depicted in Table 3 to verify the new multiport RF energy scavenging approach. It is demonstrated that the proposed rectenna system can fully exploit different frequency signals, space and polarization diversity offering broad bandwidth for scavenging RF energy from the ambient environment. The multiport and RF combining approaches offer better antenna realized gains across broadband to defeat the challenge of ambient low RF power density levels for scavenging RF energy from all available frequency ranges in the ambient atmosphere. The multiband rectifier circuit also offers excellent dc-conversion efficiency at very low RF

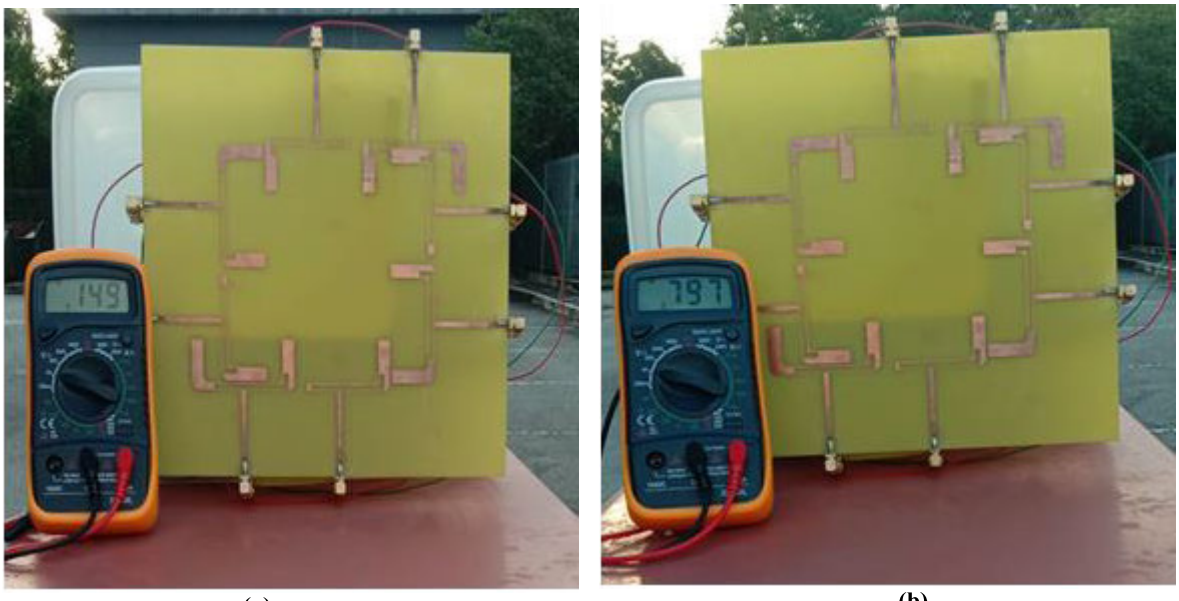

(a) (b)

FIGURE 19. Measurement in the ambient environment (a) average generated voltage per port (b) total generated voltage by the complete system.

TABLE 3. Comparative analysis of the proposed rectenna system and some prior related works.

Ref.	No. of Band	Size of Antenna (mm)	No. of Port	Combin. approach	Frequency bands, GHz	Antenna gain (dBi)	Efficiency at -20 dBm (%)
[14]	2	190×100	1	RF	1.84, 2.14	10.9, 13.3	34, 29
[29]	2	60×60	1	N/A.	0.915, 2.45	1.87, 4.18	13, 10
[33]	2	100×100	1	N/A.	2.14, 2.45	6.8, 7.6	N/A.
[70]	3	160×160	1	N/A.	2, 2.5, 3.5	7, 5.5, 9.2	20, 7, 5
[31]	4	100×100	1	N/A.	0.9, 1.8, 2.1, 2.4	6, 6, 6, 6	16, 15, 14, 14
[34]	6	160×160	1	N/A.	0.55, 0.75, 0.90, 1.85, 2.15, 2.45	2.5, 3.1, 3.6, 5.0, 5.0, 4.5	25, 20, 25,15, 9, 5
[59]	Wide	70×70	1	N/A.	1.8, 2.5	2.5, 4	33, 13
[37]	Wide	82×94	1	N/A.	0.98-1.8	2	N/A.
[71]	Wide	35×50	1	N/A.	2.4	2	15, 10
[8]	1	67×35	3	DC	1.84	3.83, 2.36, 3.9 for Port 1, 2, 3	21.1
[68]	3	175×200	2	DC	0.94, 1.84, 2.14	8.15, 7.15, 8.15	27.3, 20, 14
[64]	1	67×35.7	4	DC	1.84	3.3	21.5
[73]	1	226×337	2	DC		15.5 for Ports 1-2	N/A.
[74]	1	150×150	8	DC	2.4	Appx. 5 for Ports 1-8	28.6
[61]	1	100×60	4	Hybrid	2.45	6.6, 9.5, 9.7, 7.5 for Ports1-4	N.A.
[66]	2	240×240	16	DC	0.94, 1.84	Appx. 3.6 for Ports 1-4 Appx. 3.8 for Ports 5-16	38.1, 34
[75]	3	200×200	16	Hybrid	1.84, 2.14, 2.45	9, 11, 11	25.3, 27.9, 19.3
New	4	220×220	8	DC	0.95,1.74, 2.12, 2.42 2.90	3.2, 3.7, 3.5, 7.6, 2.9	55.5, 52.5, 66.52, 52.9, 65.5 @ -27

TABLE 4. Recorded available frequency bands and power levels (Malaysia).

Band name	Modus	Frequency Range (MHz)	Max. Power (dBm)
GSM 900	Up-link	880-915	-27.6
	Down-link	925-960	-22.5
GSM 1800	Up-link	1710-1785	-31.5
	Down-link	1805-1880	-17.8
3G	Up-link	1920-1980	-27
	Up-link	2110-2230	-23
	Down-link	2300-2360	-41.2
Wi-Fi	Up-link	2390-2400	-25.6
LTE	Down-link	2500-2700	-26.5

power density levels. Finally, it proves the benefit of the proposed multi-frequency multiport rectenna system.

C. PERFORMANCE IN AMBIENT ATMOSPHERES

In order to realize the available frequency bands with associated input RF power density levels in a semi-urban environment in Malaysia, RF spectral survey has been performed within the campus of Multimedia University, Cyberjaya. Table 4 demonstrated the verified frequency bands and corresponding input RF power density levels. To verify the proposed RF harvester's realistic performance, it is tested in ambient atmospheres (i.e. outdoor) as depicted in Figures 19 (a) and (b). The measurement is taken from the Faculty of Engineering (FOE) Garden which is situated in front of the FOE at Multimedia University (MMU), Cyberjaya, and Selangor, Malaysia. The date was 12th February at 11.30 AM. The produced dc output voltage of the multiport RF energy harvester in the outdoor ambient environment is about 0.650V and can reach 0.797V, as presented in Figure 19 (b). The generated average dc output voltage per port of the proposed rectenna is about 0.125 V and can reach 0.149 V, as depicted in Figure 19 (a). The measured dc output voltage in the outdoor ambient atmosphere is greater than that of the indoor ambient atmosphere (i.e. lab environment) since the outdoor ambient environment's RF power density is greater than that of the indoor ambient environment.

Such dc output voltage can be utilized to support small power and short duty-cycle electronic system such as sensors in IoT [31], [6], [66]. Thus, the proposed RF energy harvester is one of the practical approaches to defeat the problem of battery refilling and renewal in IoT devices.

VII. CONCLUSION

In this research, a frequency-dependent multiport rectenna system is designed and implemented for RF energy harvesting in the ambient atmosphere. The unique aspect of the suggested harvester is the ability to simultaneously exploit all available frequency bands, space coverage and spatial diversity to enhance the scavenged RF energy. Moreover, the RF combining technique is used to connect adjacent ports of the antenna structure as well as output dc voltage of all the rectifiers that are allowing extraction of RF energy at a very low input RF power density level while sustaining a wider BW for free space and frequency band coverage. The suggested RF

combining approach assisted polarization diversity by raising the amount of scavenged RF energy. Especially, the antenna part of the new harvester offers a compact 8-port broadband fork-shaped microstrip antenna with a minimal distance per port of $0.33\lambda \times 0.33\lambda$ (i.e. wavelength λ calculated at 0.9 GHz in free space) and relative BW of 35% covering the available frequency bands such as GSM 900 and 1800, 3G, Wi-Fi and LTE respectively. The insulation between two adjacent ports is larger than 16 dB and achieved a maximum realized gain of around 7 dBi. Besides, the proposed multiband rectifier with a microstrip multi-stub impedance matching network is covered for GSM 900 and 1800, 3G, Wi-Fi, and LTE frequency spectrums. The measured RF-to-dc rectification efficiency is achieved at GSM 900 and 1800, 3G, Wi-Fi and LTE frequency spectrums at very low input RF power density levels (55.5%, 52.5%, 66.52%, 52.9% and 65.5 % for -27 dBm and 44.2%, 41.2 %, 54.1%, 41.0% and 54.0% for -35 dBm). Finally, the prototype is fabricated and tested in the lab and ambient environment, illustrating that it can offer dc output voltage up to 0.797V and dc rectification efficiency is greater than 66.52% with associated RF power density level is less than of -20 dBm. Therefore, the new rectenna system is efficient for powering devices for wireless sensor networks (WSN) and the Internet of Things (IoT) as well as power management units that usually have various equivalent load resistors.

REFERENCES

[1] M. Zorzi, A. Gluhak, S. Lange, and A. Bassi, "From today's INTRAnet of things to a future Internet of Things: A wireless-and mobility-related view," *IEEE Wireless Commun.*, vol. 17, no. 6, pp. 44–51, Dec. 2010.

[2] C. Alippi and C. Galperti, "An adaptive system for optimal solar energy harvesting in wireless sensor network nodes," *IEEE Trans. Circuits Syst. I, Reg. Papers*, vol. 55, no. 6, pp. 1742–1750, Jul. 2008.

[3] F. Wei, Y. Li, Q. Sui, X. Lin, L. Chen, Z. Chen, and Z. Li, "A novel thermal energy storage system in smart building based on phase change material," *IEEE Trans. Smart Grid*, vol. 10, no. 3, pp. 2846–2857, May 2019.

[4] J. McCullagh, "An active diode full-wave charge pump for low acceleration infrastructure-based non-periodic vibration energy harvesting," *IEEE Trans. Circuits Syst. I, Reg. Papers*, vol. 65, no. 5, pp. 1758–1770, May 2018.

[5] W. C. Brown, "The history of power transmission by radio waves," *IEEE Trans. Microw. Theory Techn.*, vol. MTT-32, no. 9, pp. 1230–1242, Sep. 1984.

[6] J. A. Hagerty, F. B. Helmbrecht, W. H. McCalpin, R. Zane, and Z. B. Popovic, "Recycling ambient microwave energy with broadband rectenna arrays," *IEEE Trans. Microw. Theory Techn.*, vol. 52, no. 3, pp. 1014–1024, Mar. 2004.

[7] J. Bito, J. G. Hester, and M. M. Tentzeris, "Ambient RF energy harvesting from a two-way talk radio for flexible wearable wireless sensor devices utilizing inkjet printing technologies," *IEEE Trans. Microw. Theory Techn.*, vol. 63, no. 12, pp. 4533–4543, Dec. 2015.

[8] S. Shen, C.-Y. Chiu, and R. D. Murch, "Multiport pixel rectenna for ambient RF energy harvesting," *IEEE Trans. Antennas Propag.*, vol. 66, no. 2, pp. 644–656, Feb. 2018.

[9] A. Costanzo, M. Dionigi, D. Masotti, M. Mongiardo, G. Monti, L. Tarricone, and R. Sorrentino, "Electromagnetic energy harvesting and wireless power transmission: A unified approach," *Proc. IEEE*, vol. 102, no. 11, pp. 1692–1711, Nov. 2014.

[10] S. Kim, R. Vyas, J. Bito, K. Niotaki, A. Collado, A. Georgiadis, and M. M. Tentzeris, "Ambient RF energy-harvesting technologies for self-sustainable standalone wireless sensor platforms," *Proc. IEEE*, vol. 102, no. 11, pp. 1649–1666, Nov. 2014.

[11] N. Shinohara, "Power without wires," *IEEE Microw. Mag.*, vol. 12, no. 7, pp. S64–S73, Dec. 2011.

[12] R. Zhang and C. K. Ho, "MIMO broadcasting for simultaneous wireless information and power transfer," *IEEE Trans. Wireless Commun.*, vol. 12, no. 5, pp. 1989–2001, May 2013.

[13] M. Pinuela, P. D. Mitcheson, and S. Lucyszyn, "Ambient RF energy harvesting in urban and semi-urban environments," *IEEE Trans. Microw. Theory Techn.*, vol. 61, no. 7, pp. 2715–2726, Jul. 2013.

[14] H. Sun, Y.-X. Guo, M. He, and Z. Zhong, "A dual-band rectenna using broadband yagi antenna array for ambient RF power harvesting," *IEEE Antennas Wireless Propag. Lett.*, vol. 12, pp. 918–921, 2013.

[15] M. Arrawatia, M. S. Baghini, and G. Kumar, "Broadband rectenna array for RF energy harvesting," in *Proc. IEEE Int. Symp. Antennas Propag. (APSURSI)*, Jun. 2016, pp. 1–5.

[16] X. Wang and A. Mortazawi, "Medium wave energy scavenging for wireless structural health monitoring sensors," *IEEE Trans. Microw. Theory Techn.*, vol. 62, no. 4, pp. 1067–1073, Apr. 2014.

[17] H. Sun, Y.-x. Guo, M. He, and Z. Zhong, "Design of a high-efficiency 2.45-GHz rectenna for low-input-power energy harvesting," *IEEE Antennas Wireless Propag. Lett.*, vol. 11, pp. 929–932, 2012.

[18] M. Fantuzzi, D. Masotti, and A. Costanzo, "A novel integrated UWB–UHF one-port antenna for localization and energy harvesting," *IEEE Trans. Antennas Propag.*, vol. 63, no. 9, pp. 3839–3848, Sep. 2015.

[19] D. De Donno, L. Catarinucci, and L. Tarricone, "An UHF RFID energy-harvesting system enhanced by a DC-DC charge pump in Silicon-on-Insulator technology," *IEEE Microw. Wireless Compon. Lett.*, vol. 23, no. 6, pp. 315–317, Jun. 2013.

[20] R. Colella, L. Tarricone, and L. Catarinucci, "SPARTACUS: Self-powered augmented RFID tag for autonomous computing and ubiquitous sensing," *IEEE Trans. Antennas Propag.*, vol. 63, no. 5, pp. 2272–2281, May 2015.

[21] S. D. Assimonis, S.-N. Daskalakis, and A. Bletsas, "Sensitive and efficient RF harvesting supply for batteryless backscatter sensor networks," *IEEE Trans. Microw. Theory Techn.*, vol. 64, no. 4, pp. 1327–1338, Apr. 2016.

[22] A. Georgiadis, G. Vera Andia, and A. Collado, "Rectenna design and optimization using reciprocity theory and harmonic balance analysis for electromagnetic (EM) energy harvesting," *IEEE Antennas Wireless Propag. Lett.*, vol. 9, no. 4, pp. 444–446, May 2010.

[23] M. Arrawatia, M. S. Baghini, and G. Kumar, "Differential microstrip antenna for RF energy harvesting," *IEEE Trans. Antennas Propag.*, vol. 63, no. 4, pp. 1581–1588, Apr. 2015.

[24] F. Xie, G.-M. Yang, and W. Geyi, "Optimal design of an antenna array for energy harvesting," *IEEE Antennas Wireless Propag. Lett.*, vol. 12, pp. 155–158, 2013.

[25] D. Ferreira, L. Sismeiro, A. Ferreira, R. F. S. Caldeirinha, T. R. Fernandes, and I. Cuinas, "Hybrid FSS and rectenna design for wireless power harvesting," *IEEE Trans. Antennas Propag.*, vol. 64, no. 5, pp. 2038–2042, May 2016.

[26] T. Peter, T. A. Rahman, S. W. Cheung, R. Nilavalan, H. F. Abutarboush, and A. Vilches, "A novel transparent UWB antenna for photovoltaic solar panel integration and RF energy harvesting," *IEEE Trans. Antennas Propag.*, vol. 62, no. 4, pp. 1844–1853, Apr. 2014.

[27] H. Kanaya, S. Tsukamaoto, T. Hirabaru, D. Kanemoto, R. K. Pokharel, and K. Yoshida, "Energy harvesting circuit on a one-sided directional flexible antenna," *IEEE Microw. Wireless Compon. Lett.*, vol. 23, no. 3, pp. 164–166, Mar. 2013.

[28] R. J. Vyas, B. B. Cook, Y. Kawahara, and M. M. Tentzeris, "E-WEHP: A batteryless embedded sensor-platform wirelessly powered from ambient digital-TV signals," *IEEE Trans. Microw. Theory Techn.*, vol. 61, no. 6, pp. 2491–2505, Jun. 2013.

[29] K. Niotaki, S. Kim, S. Jeong, A. Collado, A. Georgiadis, and M. M. Tentzeris, "A compact dual-band rectenna using slot-loaded dual band folded dipole antenna," *IEEE Antennas Wireless Propag. Lett.*, vol. 12, pp. 1634–1637, 2013.

[30] H. Kamoda, S. Kitazawa, N. Kukutsu, and K. Kobayashi, "Loop antenna over artificial magnetic conductor surface and its application to dual-band RF energy harvesting," *IEEE Trans. Antennas Propag.*, vol. 63, no. 10, pp. 4408–4417, Oct. 2015.

[31] V. Kuhn, C. Lahuec, F. Seguin, and C. Person, "A multi-band stacked RF energy harvester with RF-to-DC efficiency up to 84%," *IEEE Trans. Microw. Theory Techn.*, vol. 63, no. 5, pp. 1768–1778, May 2015.

[32] K. Niotaki, A. Georgiadis, A. Collado, and J. S. Vardakas, "Dual-band resistance compression networks for improved rectifier performance," *IEEE Trans. Microw. Theory Techn.*, vol. 62, no. 12, pp. 3512–3521, Dec. 2014.

[33] S. Shen, C. Y. Chiu, and R. D. Murch, "A broadband L-probe microstrip patch rectenna for ambient RF energy harvesting," in *Proc. IEEE Int. Symp. Antennas Propag. USNC/URSI Nat. Radio Sci. Meeting*, Jul. 2017, pp. 2037–2038.
[34] C. Song, Y. Huang, P. Carter, J. Zhou, S. Yuan, Q. Xu, and M. Kod, "A novel six-band dual CP rectenna using improved impedance matching technique for ambient RF energy harvesting," *IEEE Trans. Antennas Propag.*, vol. 64, no. 7, pp. 3160–3171, Jul. 2016.
[35] H. Saghlatoon, T. Bjorninen, L. Sydanheimo, M. M. Tentzeris, and L. Ukkonen, "Inkjet-printed wideband planar monopole antenna on cardboard for RF energy-harvesting applications," *IEEE Antennas Wireless Propag. Lett.*, vol. 14, pp. 325–328, 2015.
[36] C. Song, Y. Huang, J. Zhou, J. Zhang, S. Yuan, and P. Carter, "A high-efficiency broadband rectenna for ambient wireless energy harvesting," *IEEE Trans. Antennas Propag.*, vol. 63, no. 8, pp. 3486–3495, Aug. 2015.
[37] M. Arrawatia, M. Shojaei Baghini, and G. Kumar, "Broadband bent triangular omnidirectional antenna for RF energy harvesting," *IEEE Antennas Wireless Propag. Lett.*, vol. 15, pp. 36–39, 2016.
[38] J. O. McSpadden and K. Chang, "A dual polarized circular patch rectifying antenna at 2.45 GHz for microwave power conversion and detection," in *IEEE MTT-S Int. Microw. Symp. Dig.*, vol. 3, May 1994, pp. 1749–1752.
[39] Z. Popoviá, S. Korhummel, S. Dunbar, R. Scheeler, A. Dolgov, R. Zane, E. Falkenstein, and J. Hagerty, "Scalable RF energy harvesting," *IEEE Trans. Microw. Theory Techn.*, vol. 62, no. 4, pp. 1046–1056, Apr. 2014.
[40] H. Sun and W. Geyi, "A new rectenna with all-polarization-receiving capability for wireless power transmission," *IEEE Antennas Wireless Propag. Lett.*, vol. 15, pp. 814–817, 2016.
[41] Z. Harouni, L. Cirio, L. Osman, A. Gharsallah, and O. Picon, "A dual circularly polarized 2.45-GHz rectenna for wireless power transmission," *IEEE Antennas Wireless Propag. Lett.*, vol. 10, pp. 306–309, 2011.
[42] J.-H. Chou, D.-B. Lin, K.-L. Weng, and H.-J. Li, "All polarization receiving rectenna with harmonic rejection property for wireless power transmission," *IEEE Trans. Antennas Propag.*, vol. 62, no. 10, pp. 5242–5249, Oct. 2014.
[43] T.-C. Yo, C.-M. Lee, C.-M. Hsu, and C.-H. Luo, "Compact circularly polarized rectenna with unbalanced circular slots," *IEEE Trans. Antennas Propag.*, vol. 56, no. 3, pp. 882–886, Mar. 2008.
[44] F.-J. Huang, T.-C. Yo, C.-M. Lee, and C.-H. Luo, "Design of circular polarization antenna with harmonic suppression for rectenna application," *IEEE Antennas Wireless Propag. Lett.*, vol. 11, pp. 592–595, 2012.
[45] H. Takhedmit, L. Cirio, S. Bellal, D. Delcroix, and O. Picon, "Compact and efficient 2.45 GHz circularly polarised shorted ring-slot rectenna," *Electron. Lett.*, vol. 48, no. 5, pp. 253–254, Mar. 2012.
[46] X.-X. Yang, C. Jiang, A. Z. Elsherbeni, F. Yang, and Y.-Q. Wang, "A novel compact printed rectenna for data communication systems," *IEEE Trans. Antennas Propag.*, vol. 61, no. 5, pp. 2532–2539, May 2013.
[47] Z. Ma and G. A. E. Vandenbosch, "Wideband harmonic rejection filtenna for wireless power transfer," *IEEE Trans. Antennas Propag.*, vol. 62, no. 1, pp. 371–377, Jan. 2014.
[48] T. S. Almoneef, H. Sun, and O. M. Ramahi, "A 3-D folded dipole antenna array for far-field electromagnetic energy transfer," *IEEE Antennas Wireless Propag. Lett.*, vol. 15, pp. 1406–1409, 2016.
[49] B. Strassner and K. Chang, "Highly efficient c-band circularly polarized rectifying antenna array for wireless microwave power transmission," *IEEE Trans. Antennas Propag.*, vol. 51, no. 6, pp. 1347–1356, Jun. 2003.
[50] Y.-J. Ren and K. Chang, "5.8-GHz circularly polarized dual-diode rectenna and rectenna array for microwave power transmission," *IEEE Trans. Microw. Theory Techn.*, vol. 54, no. 4, pp. 1495–1502, Jun. 2006.
[51] T. Sakamoto, Y. Ushijima, E. Nishiyama, M. Aikawa, and I. Toyoda, "5.8-GHz Series/Parallel connected rectenna array using expandable differential rectenna units," *IEEE Trans. Antennas Propag.*, vol. 61, no. 9, pp. 4872–4875, Sep. 2013.
[52] T. Matsunaga, E. Nishiyama, and I. Toyoda, "5.8-GHz stacked differential rectenna suitable for large-scale rectenna arrays with DC connection," *IEEE Trans. Antennas Propag.*, vol. 63, no. 12, pp. 5944–5949, Dec. 2015.
[53] A. Massa, G. Oliveri, F. Viani, and P. Rocca, "Array designs for long-distance wireless power transmission: State-of-the-art and innovative solutions," *Proc. IEEE*, vol. 101, no. 6, pp. 1464–1481, Jun. 2013.
[54] U. Olgun, C. C. Chen, and J. L. Volakis, "Investigation of rectenna array configurations for enhanced RF power harvesting," *IEEE Antennas Wireless Propag. Lett.*, vol. 10, no. 4, pp. 262–265, Apr. 2011.
[55] J. W. Wallace and M. A. Jensen, "Mutual coupling in MIMO wireless systems: A rigorous network theory analysis," *IEEE Trans. Wireless Commun.*, vol. 3, no. 4, pp. 1317–1325, Jul. 2004.
[56] S. Shen and R. D. Murch, "Impedance matching for compact multiple antenna systems in random RF fields," *IEEE Trans. Antennas Propag.*, vol. 64, no. 2, pp. 820–825, Feb. 2016.
[57] J. Y. Sze and K. L. Wong, "Bandwidth enhancement of a microstrip-line-fed printed wide-slot antenna," *IEEE Trans. Antennas Propag.*, vol. 49, no. 7, pp. 1020–1024, Jul. 2001.
[58] M. R. Ghaderi and F. Mohajeri, "A compact hexagonal wide-slot antenna with microstrip-fed monopole for UWB application," *IEEE Antennas Wireless Propag. Lett.*, vol. 10, no. 4, pp. 682–685, May 2011.
[59] S. R. Emadian and J. A. Shokouh, "Very small dual band-notched rectangular slot antenna with enhanced impedance bandwidth," *IEEE Trans. Antennas Propag.*, vol. 63, no. 10, pp. 4529–4534, Oct. 2015.
[60] D.-J. Lee, S.-J. Lee, I.-J. Hwang, W.-S. Lee, and J.-W. Yu, "Hybrid power combining rectenna array for wide incident angle coverage in RF energy transfer," *IEEE Trans. Microw. Theory Techn.*, vol. 65, no. 9, pp. 3409–3418, Sep. 2017.
[61] S. Shen, Y. Zhang, C.-Y. Chiu, and R. D. Murch, "Compact quad-port dual-polarized dipole rectenna for ambient RF energy harvesting," in *Proc. 12th Eur. Conf. Antennas Propag. (EuCAP)*, 2018, pp. 1–5.
[62] A. J. S. Boaventura, A. Collado, A. Georgiadis, and N. B. Carvalho, "Spatial power combining of multi-sine signals for wireless power transmission applications," *IEEE Trans. Microw. Theory Techn.*, vol. 62, no. 4, pp. 1022–1030, Apr. 2014.
[63] S. Shen, Y. Zhang, C.-Y. Chiu, and R. Murch, "An ambient RF energy harvesting system where the number of antenna ports is dependent on frequency," *IEEE Trans. Microw. Theory Techn.*, vol. 67, no. 9, pp. 3821–3832, Sep. 2019.
[64] C. A. Balanis, *Antenna Theory and Design*. New York, NY, USA: Wiley, 2012.
[65] S. Shen, C.-Y. Chiu, and R. D. Murch, "A dual-port triple-band L-probe microstrip patch rectenna for ambient RF energy harvesting," *IEEE Antennas Wireless Propag. Lett.*, vol. 16, pp. 3071–3074, 2017.
[66] A. E. Abdulhadi and R. Abhari, "Multiport UHF RFID-tag antenna for enhanced energy harvesting of self-powered wireless sensors," *IEEE Trans. Ind. Electron.*, vol. 12, no. 2, pp. 801–808, Apr. 2016.
[67] S. Chandravanshi, S. S. Sarma, and M. J. Akhtar, "Design of triple band differential rectenna for RF energy harvesting," *IEEE Trans. Antennas Propag.*, vol. 66, no. 6, pp. 2716–2726, Jun. 2018.
[68] Y. Shi, Y. Fan, Y. Li, L. Yang, and M. Wang, "An efficient broadband slotted rectenna for wireless power transfer at LTE band," *IEEE Trans. Antennas Propag.*, vol. 67, no. 2, pp. 814–822, Feb. 2019.
[69] Y.-Y. Hu, S. Sun, H. Xu, and H. Sun, "Grid-array rectenna with wide angle coverage for effectively harvesting RF energy of low power density," *IEEE Trans. Microw. Theory Techn.*, vol. 67, no. 1, pp. 402–413, Jan. 2019.
[70] Y. Zhang, "Hybrid RF-solar energy harvesting systems utilizing transparent multiport micromeshed antennas," *IEEE Trans. Microw. Theory Techn.*, vol. 67, no. 11, pp. 4534–4546, Nov. 2019.
[71] S. Shen, Y. Zhang, C.-Y. Chiu, and R. Murch, "A triple-band high-gain multibeam ambient RF energy harvesting system utilizing hybrid combining," *IEEE Trans. Ind. Electron.*, vol. 67, no. 11, pp. 9215–9226, Nov. 2020.

SUNANDA ROY (Graduate Student Member, IEEE) received the B.Sc. degree in electronics and communication engineering (ECE) from Khulna University, Bangladesh, and the Master of Engineering degree in electrical and electronic engineering (EEE) from the Khulna University of Engineering and Technology (KUET), Bangladesh. He is currently pursuing the Ph.D. degree with the Faculty of Engineering (FOE), Multimedia University (MMU), Malaysia, under TM Research and Development Research Grant. His research interests include ambient RF energy harvesting, hybrid harvesting, MIMO, multiband antenna design, integrated circuit design, and amplifier design.

R. JUN-JIAT TIANG received the bachelor's degree in electronics engineering from Multimedia University, Malaysia, the master's degree from the University of Science, Malaysia, and the Ph.D. degree from the Universiti Kebangsaan Malaysia (UKM). He was worked as an Electronics Engineer with the Global Technology Development Group, Motorola Technology Sdn. Bhd., Malaysia, from May 2006 to May 2007, and a Design Automation Engineer with the Chipset Structural Design Team, Intel Microelectronics (M) Sdn. Bhd., Malaysia, from September 2004 to July 2005. He is currently a Senior Lecturer and a Researcher with the Faculty of Engineering, Multimedia University. He has vast experience while working as a Project Leader in various research grants, such as Technology and Innovation (MOSTI), from 2008 to 2010; Research Grant Mini Fund, in 2016; and TM Research and Development Research Grant, Ministry of Science, from 2017 to 2020. His interests include RFID, microwave circuits, antenna, and propagation. He was awarded the Gold Medal at the 23rd International Invention, Innovation and Technology Exhibition (ITEX) 2012, Kuala Lumpur, Malaysia, in May 2012; and the Silver Medal at the Malaysian Technology Expo (MTE) 2013, Kuala Lumpur, in February 2013.

MARDENI BIN ROSLEE (Senior Member, IEEE) is currently working as an Associate Professor with the Research Institute of Digital Connectivity and the Faculty of Engineering, Multimedia University, Cyberjaya, Malaysia. He is also the President of MMU Mesra and the Chairman of the Centre of Wireless Technology. At the international level, he is also the Chairman of Malaysia IEEE Comsoc/VTS, and the Head of the Malaysian Radar and Navigations Interest Group (MyRaN ig), the Malaysian Society for Engineering and Technology (MY SET), which is for recognized and selected members in a professional organization, networking, interaction with like-minded multidisciplinary professionals from public and private sectors, and the international platforms in the 21st century. He is also the Chief Executive Officer (CEO) and the Founder of Armada Company Ltd. He is also the Keynote Speaker for IEEE SOFTT19 and I3CPE'19. He is also a registered Chartered Engineer with the Engineering Council, U.K., and a member of The Institution of Engineering and Technology (IET), U.K. As a Chartered Engineer, he brings a diversified range of engineering experience in design and development and engineering management. At the national and international level, he has been involved in industry consultation and collaborations with some companies, private and government sectors, such as TM, Celcom, Webe Digital, TM, FCE Nigeria, Tashmanbet Bagdat Erlanuly, Kazakhstan, Mimos Bhd, Sony EMCS, Plexus Sdn. Bhd., Aexio Sdn. Bhd., MDEC, Innocrest Enterprise, Ministry of Housing and Local Government, MAMPU, and WCC Telco. His experiences include the consultation, professional institution, and academic sectors. His current research interests include 5G/6G telecommunication, D2D, satellite, the Internet of Things, and radar communication. His contributions to academic and engineering professional over the years have earned him recognitions nationally and internationally, he has awarded 26 international/local awards, including the University Excellent Researcher Award, in 2016 and 2018; the VTS Chapter of the Year Award, the 2017 IEEE 86th VTC2017-Fall, Toronto, Canada, in September 2017; the Excellence in European Creativity Special Award, in 2018; and the World Invention Special Award, in 2019. He has been invited by IEEE International Conference, as a Session Chair, such as in Thailand, China, Japan, Korea, Australia, and Turkey. He has held some international conference committees, such as the Conference Co-Chair of IEEE MICC2019; committees for IEEE ISTT18, IEEE MICC17, and IEEE ISTT16; and a TPC for IEEE MENACOMM'19 Bahrain, IEEE PIMRC 2019 Turkey, IEEE PIMRC 2018 Italy, IEEE PIMRC 2017 Canada, IEEE PIMRC 2016 Spain, and IEEE PIMRC 2015 Hong Kong.

MD. TANVIR AHMED (Student Member, IEEE) received the B.Eng. degree from Multimedia University, Cyberjaya. He researched with the Advanced EM Lab, Multimedia University. He has co-organized more than 30 workshops, industrial tours, and webinars under the banner of the IEEE MMU Student Branch. He worked as the Secretariat of the IEEE Malaysia Annual General Meeting, in 2018. He is currently working as an Engineer Intern with Keysight Technologies, Malaysia. His research interests include multiband antenna, RF energy harvesting, hybrid energy harvesting, solar, the embedded IoT, and machine learning. Throughout his academic life, he received four prestigious Government MERIT Scholarships along with several awards for outstanding academic performances.

M. A. PARVEZ MAHMUD received the B.Sc. degree in electrical and electronic engineering, the Master of Engineering degree in mechatronics engineering, and the Ph.D. degree. After the successful completion of his Ph.D. degree with multiple awards, he worked as a Postdoctoral Research Associate and Academic in the School of Engineering at Macquarie University, Sydney. He worked with the World University of Bangladesh (WUB), as a Lecturer for more than two years and the Korea Institute of Machinery and Materials (KIMM), as a Researcher for about three years. He is currently an Alfred Deakin Postdoctoral Research Fellow with Deakin University. He is also a Key Member of Deakin University's Advanced Integrated Microsystems (AIM) Research Group. He was involved in teaching engineering subjects in the electrical, biomedical, and mechatronics engineering courses with the School of Engineering, Macquarie University, for more than two years. He is also involved in the supervision of six Ph.D. students with Deakin University. Apart from this, he is also actively involved with different professional organizations, including Engineers Australia and IEEE. He accumulated experience and expertise in machine learning, life cycle assessment, sustainability and economic analysis, materials engineering, microfabrication, and nanostructured energy materials to facilitate technological translation from the lab to real-world applications for a better society. He has produced over 50 publications, including one authored book, three book chapters, 29 journal articles, and 21 fully refereed conference papers. His research interests include energy sustainability, secure energy trading, micro grid control and economic optimization, machine learning, data science, and micro/nanoscale technologies for sensing and energy harvesting. He received several awards, including the Macquarie University Highly Commended Excellence in Higher Degree Research Award, in 2019.